Engineering Structures 304 (2024) 117575

Contents lists available at ScienceDirect

Engineering Structures

journal homepage: www.elsevier.com/locate/engstruct

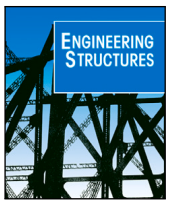

Aleatoric and epistemic uncertainty in the overstrength of CLT-to-CLT screwed connections

Angelo Aloisio [a,b,*], Yuri De Santis [a], Dag Pasquale Pasca [c], Massimo Fragiacomo [a], Roberto Tomasi [b]

[a] Department of Civil, Construction-Architectural and Environmental Engineering , Università degli Studi dell'Aquila, L'Aquila, 67100, Italy
[b] Faculty of Science and Technology, Norwegian University of Life Sciences, Norway
[c] Norsk Treteknisk Institutt (Norwegian Institute of Wood Technology), Børrestuveien 3, 0373 Oslo, Norway

ARTICLE INFO

Keywords:
Overstrength
Cross-laminated timber
Screw connections
Uncertainty quantification

ABSTRACT

The most common and practical connection between CLT walls can be realized with inclined screws. This choice avoids the realization of more elaborated half-lap or spline joints. The failure mechanism of CLT-to-CLT screwed connections is highly ductile. However, the epistemic and aleatoric uncertainties associated with the capacity estimation of the connection might lead to an undesired overstrength, compromising the expected hierarchy between failure mechanisms. This paper presents the results of an extended experimental campaign to estimate the overstrength of CLT-to-CLT screwed connections. However, the overstrength directly obtained from the experimental tests could be underestimated. In the experimental campaign, the same wood and screw stock is used, which might not represent the actual scatter of the material properties and construction uncertainties of the as-built connection (e.g., the screw inclination). Therefore, this paper attempts to provide a model-driven assessment of the overstrength factor, assuming more realistic values for the parameter uncertainties. The authors propose a method for removing the contribution of epistemic uncertainty to the model-driven estimation of the overstrength based on experimental tests with two Montecarlo simulations. Following the proposed method, the paper compares the overstrength estimations from the experimental tests to the predictions of analytical and nonlinear finite element models. This study has proven that an overstrength factor between 1.8 and 2 can represent the actual uncertainties in as-built CLT-to-CLT screwed connections.

1. Introduction

Capacity-based design methods are standard in structural engineering and have been introduced in the current design codes, like the Eurocode 8 [2,3]. The ductility of timber structures during a seismic event depends on the ductility of the connections [4–6]. In mass timber structures constructed in seismic regions, well-detailed connections should provide ductility and energy dissipation under seismic loading, while the mass timber elements should remain elastic. This ductility can be achieved using any fastener plasticization, timber crushing, or novel friction or damping devices [7–9].

However, not all connections possess the same level of ductility. Therefore, to achieve a highly ductile seismic response, it is essential to guarantee a specific hierarchy among failure mechanisms [10]. The most ductile failure mechanisms should occur before the brittle ones. However, the uncertainty associated with the capacity estimate and the material properties might lead to an undesired overstrength of the ductile connections. Therefore, the undesired higher capacity of the more ductile connections might cause the less ductile connection to fail before the more ductile one. Therefore, designing less ductile connections with a certain overstrength is crucial to achieving the desired hierarchy of failure mechanisms.

The first and most successful formulation for predicting the overstrength of timber connections was proposed by Fragiacomo and Jorissen [11]. This formulation comprises the two sources of uncertainty in the overstrength, the epistemic and aleatoric, related to the adopted capacity formulation and the intrinsic scatter of the material properties, respectively. The scientific literature confirmed the high success of this formulation. Almost all scientific papers presenting

* Corresponding author at: Department of Civil, Construction-Architectural and Environmental Engineering , Università degli Studi dell'Aquila, L'Aquila, 67100, Italy.
E-mail addresses: angelo.aloisio1@univaq.it (A. Aloisio), yuri.desantis@univaq.it (Y. De Santis), dpa@treteknisk.no (D.P. Pasca), massimo.fragiacomo@univaq.it (M. Fragiacomo), roberto.tomasi@nmbu.no (R. Tomasi).

https://doi.org/10.1016/j.engstruct.2024.117575
Received 1 March 2023; Received in revised form 19 May 2023; Accepted 26 January 2024
Available online 9 February 2024

List of symbols and notation

Latin letters

a_1	Distance between two screws in the direction parallel to the grain;
a_{3c}	Distance between the screw and the panel edge in the direction parallel to the grain;
a_{3t}	Distance between the screw and the panel edge in the direction orthogonal to the grain;
b	Ratio between embedment stiffness perpendicular to the grain and embedment stiffness parallel to the grain;
D_{exp}	Experimental ductility ratio, estimated as the ratio between the ultimate ($v_{u,exp}$) and yielding ($v_{y,exp}$) displacements.
d	Nominal diameter of the screw;
d_{ef}	Effective diameter of the screw;
d_{core}	Inner diameter of the screw;
E	Expected value operator;
$F_{y,exp}$	Experimental yielding force estimated at the intersection between the lines associated with the elastic ($k_{el,exp}$) and plastic ($k_{pl,exp}$) stiffness.
$F_{u,exp}$	Ultimate experimental force estimated following the EN:12512;
$F_{max,exp}$	Maximum experimental force;
$F_{ax,Rk}$	Characteristic axial capacity of the fastener;
$f_{h,k}$	Characteristic embedment strength of the screw. The subscripts 1 ($f_{h,1,k}$) and 2 ($f_{h,2,k}$) indicate the embedment strength of the first and second timber components of the connection;
$f_{h,\alpha}$	Mean embedment strength of the screw at an angle α to the grain;
$f_{h,0}$	Mean embedment strength of the screw parallel to the grain;
f_y	Characteristic yielding strength of steel;
$f_{y,m}$	Mean yielding strength of steel;
l_{ef}	Effective screw penetration depth in mm.
k	Epistemic correction factor in Eq. (17);
$k_{90,e}$	1.35 + 0.015d according to the EC5;
$k_{el,exp}$	Elastic stiffness of the experimental force–displacement curve according to the EN:125129;
$k_{pl,exp}$	Plastic stiffness of the experimental force–displacement curve according to the Y & K method [1];
$k_{h,0}$	Embedment stiffness per unit length parallel to the grain direction;
$k_{h,90}$	Embedment stiffness per unit length perpendicular to the grain direction;
m	Friction coefficient;
m_m	Mean friction coefficient;
$M_{y,Rk}$	Characteristic yielding moment of the fastener;
$\mathcal{N}$	Normal probability density function;
n	Number of experimental tests;
$\hat{p}_f$	Target failure probability;
$R_{v,k}$	Characteristic shear capacity of the single screw;
R_{brt}	Capacity of a brittle failure mechanism;
$R_{\text{dct,exp}}$	Capacity of a ductile failure mechanism estimated from experimental data;
$R_{\text{dct,exp},m}$	Mean capacity of a ductile failure mechanism estimated from experimental data;
$R_{\text{dct,exp},0.95}$	0.95 quantiles of the capacity of a ductile failure mechanism estimated from experimental tests;
$R_{\text{dct,exp},0.05}$	0.05 quantile of the capacity of a ductile failure mechanism estimated from experimental tests;
$R_{\text{dct,an},k}$	Characteristic capacity of a ductile failure mechanism estimated from an analytical capacity model;
$R_{\text{dct,an},d}$	Design capacity of a ductile failure mechanism estimated from an analytical capacity model;
$R_{\text{dct,mod}}$	Capacity of a ductile failure mechanism estimated from a capacity model;
t_1 and t_2	Penetration lengths of the screws in the first and second timber element of the connection;
$v_{y,exp}$	Experimental yielding displacement, found at the intersection between the lines associated with the elastic ($k_{el,exp}$) and plastic ($k_{pl,exp}$) displacements;
$v_{u,exp}$	Experimental ultimate displacement, which is the displacement corresponding to $F_{u,exp}$; $\boldsymbol{x}$ Model parameters; $\boldsymbol{x}_{\text{exp}}$ Model parameters representative of the experimental tests;

Greek letters

α	Angle in radians between the screw and grain directions in the outer layer.
α_m	Angle in radians between the screw and grain directions in the outer layer.
β	Reliability index;
γ	Ratio between $f_{h,1,k}$ and $f_{h,2,k}$.
γ_{Rd}	Overstrength factor;
γ^*_{Rd}	Partial overstrength factor;
$\gamma^*_{Rd,\text{mod}}$	Model-driven partial overstrength factor in Eq. (19);
γ_{sc}	Contribution to overstrength of the scatter of the experimental data;
γ_{an}	Contribution to overstrength of the error of the analytical model;
γ_M	Partial safety factor;
$\mathcal{E}$	Model error defined as the difference between the experimental and analytical capacity;
$\mathcal{E}_{\text{epi}}$	Epistemic uncertainty;
$\mathcal{E}_{\text{al}}$	aleatoric uncertainty;
θ	Coefficient of variation;
$\boldsymbol{\Theta}$	Uncertainty of the model parameters;
$\boldsymbol{\Theta}_{\text{exp}}$	Uncertainty of the model parameters representative of the experimental tests;
μ	Mean of a Normal probability density function;
μ_{epi}	Epistemic bias;
ρ	Wood density
ρ_m	Mean wood density
$\rho_{B,k}$	Characteristic bulk density of wood;
σ_{exp}	Standard deviation of the capacity values obtained from the experimental tests;

experimental test results estimate the overstrength using the formulation proposed by Jorissen & Fragiacomo. The definition of the overstrength factor according to Jorissen A. & Fragiacomo M., 2011 [11] is:

$$\gamma_{\text{Rd}} = \frac{R_{\text{dct,exp},0.95}}{R_{\text{dct,an},d}} = \frac{R_{\text{dct,exp},0.95}}{R_{\text{dct,exp},0.05}} \cdot \frac{R_{\text{dct,exp},0.05}}{R_{\text{dct,an},k}} \cdot \frac{R_{\text{dct,an},k}}{R_{\text{dct,an},d}} = \gamma_{sc} \cdot \gamma_{an} \cdot \gamma_M \quad (1)$$

σ_{epi}	Standard deviation of a Normal probability density function representative of the epistemic model error;
σ_{al}	Standard deviation of a Normal probability density function representative of the aleatoric model error;
σ_{mod}	Standard deviation of a Normal probability density function representative of the total error;

Acronyms

CLT	Cross Laminated Timber
CoV	Coefficient of variation;
CoV_{fy}	Coefficient of the steel strength;
CoV_m	Coefficient of the friction coefficient;
CoV_ρ	Coefficient of the wood density;
CoV_α	Coefficient of the angle between the screw and the grain direction of the outer layer of the CLT panel;
FE	Finite Element
Std. Dev.	Standard deviation;

where $R_{dct,exp,0.95}$ and $R_{dct,exp,0.05}$ are respectively the 95th and 5th percentile of the ductile component capacity distribution; $R_{dct,an,k}$ and $R_{ductile,an,d}$ are respectively the characteristic and the design values of the analytical prediction of the ductile element capacity. The coefficient γ_{sc} expresses the scatter of the experimental connection strength properties indicating the reliability of the connection. The coefficient γ_{an} expresses the approximation of the analytical formula used to evaluate the strength property. Finally, γ_M is the partial material factor. Based on this definition, Jorissen & Fragiacomo derived overstrength values from 1.20 to 1.85 for dowelled connections [11].

The advantages of the formulation in Eq. (1) are clarity and ease of implementation. The formulation falls within the so-called semi-probabilistic methods. The main flaw of the equation is the lack of a solid reliability-based foundation. The lack of reliability-based approaches in estimating overstrength in many scientific papers depends on two concurring factors. The reliability-based methods require formulating a limit state function in terms of ductile and brittle failure mechanisms, which cannot be generally solved analytically and require an empirical approach based on Montecarlo simulations. The second aspect relates to the first. Estimating the overstrength from the test results cannot be generally formulated as a limit state function since a single failure mechanism is often observed. Therefore, this fact undermines the application of reliability-based approaches for assessing the overstrength of timber connections from experimental tests.

Few papers deal with the overstrength of timber connections, and most present the results of experimental tests used to assess the overstrength from Eq. (1), see [11,12]. Jorissen and Fragiacomo [11] studied the overstrength of timber-to-timber dowelled connections. Schick et al. [12] carried out monotonic tests for shear parallel to the grain [12] to estimate the overstrength of nails and staples in light-frame timber panels (OSB, GFB).

Most research papers on overstrength in timber engineering have recently focused on Cross-Laminated Timber (CLT) buildings. The reason for this interest is the increasing spreading of CLT buildings in seismic-prone areas and the need to understand further and evaluate the role of overstrength in their seismic response [13]. Overstrength is crucial in capacity design at four levels: (1) structural, (2) assembly, (3) fastener and (4) connection. Most papers present the experimental evaluation of overstrength in CLT building at a connection level, neglecting the higher levels [14]. However, in design, following the resistance hierarchy principle at all levels is crucial. Specifically, in the case of CLT buildings, the possibly favoured failure mechanism should be the rocking and the sliding due to higher ductility. At the structural level, the dissipation should occur within wall-to-foundation, wall-to-floor, and vertical wall-to-wall connection lines [13,15]. The designer must ensure adequate ductility in these regions, while the other should remain in the elastic range during seismic excitation. CLT has much higher strength and stiffness than traditional light timber-framed (LTF) assemblies [13], often applied in low-rise or mid-rise residential construction. However, while CLT lends itself well to many applications, its structural performance has often been hampered by the lack of efficient connection systems. For example, in the seismic design of CLT shear walls, engineers frequently specify off-the-shelf brackets (hold-downs, shear keys) initially developed for LTF buildings [4,16,17].

A leading ductile mechanism in CLT buildings is associated with the dissipation between adjacent walls. The most common connection system between CLT walls is obtained with inclined screws [18,19]. This solution avoids the more elaborated half-lap or spline joints; see Fig. 1. Recently, researchers have been investigating mixed angle screwed (MAS) connections as alternative stronger and stiffer connection systems for high-capacity CLT shear wall applications [20,21].

While there has been intense research interest in understanding CLT shear wall behaviour, both at the connection level [4,5,22–27] and system level [4,28–31], no paper has presented an extended experimental assessment of the overstrength in CLT-to-CLT screw connections. Below, the authors provide a short review of the research papers dealing with the overstrength of CLT connections. Sustersic [32] estimated the overstrength on nailed hold-downs and angle brackets in CLT panels, using Eq. (1). The γ_{Rd} was approximately 1.3. Fragiacomo evaluated the overstrength of timber-to-timber screwed connections between orthogonal CLT panels [33] under cyclic shear obtaining overstrength values equal to 1.6. Gavric et al. tested screwed connections between CLT panels [34] under cyclic shear and angle brackets (nailed to CLT panels [24], obtaining an overstrength ranging between 1.2 and 1.9. Krauss et al. [35] assessed the influence of mixed-angle screw installations in CLT on the cyclic performance of commercial hold-down connections. The obtained overstrength ranged between 3.2 and 1.9.

The only paper dealing with the overstrength of screwed CLT-to-CLT screwed connection is the one by Gavric et al. [34]. However, this paper only considers the lap or spline joint, not the typical configuration based on inclined screws, case (c) in Fig. 1.

Additionally, as discussed by [14], no paper provides a probabilistic assessment of overstrength. The only paper following a reliability-based approach is the one by [36] on dowelled connection. With a reliability target equal to $\beta = 3.8$, they obtained a γ_{Rd} equal to 1.99. Brühl et al. [37] investigated moment-resistant connections in GLT beams and used Monte Carlo (MC) simulations (108 repetitions).

The research group of Prof. Tannert has contributed to understanding shear connections between CLT panels using inclined screws. Their research primarily focuses on experimental testing to characterize the behaviour of screwed connections in CLT panels. However, their work lacks advanced connection modelling and a discussion of the uncertainty propagation of model parameters on capacity estimation. Namely, Brown et al. [38] investigated orthogonal joints between CLT panels, aiming to develop enhanced joints for CLT wall panels. They conducted monotonic and cyclic loading tests on 59 specimens with varying combinations of mixed-angle steel-to-steel (STS) connections. The study evaluated strength, displacement capacity, ductility, stiffness, and overstrength but did not involve finite element (FE) modelling of the connections. Overstrength assessment relied on a conventional formulation. Hossain et al. (2016) [39] examined fully threaded STS assemblies with a double inclination of fasteners for in-plane shear force transfer between CLT panels. They performed quasi-static monotonic and reversed cyclic loading tests on ten three-panel CLT specimens with two shear planes each. The results provided

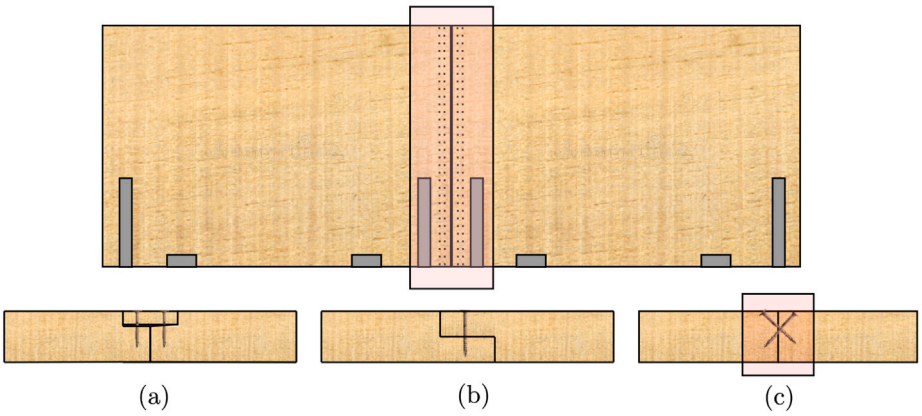

Fig. 1. Possible ways to connect two adjacent parallel panels in a segmented CLT shear wall.

data on connection yield load, yield displacement, capacity, stiffness, and ductility ratio. However, the study lacks an interpretative capacity model for the experimental data. Loss et al. [40] investigated the performance of simple CLT shear connections using butt joints and various spatial arrangements of STS. They tested 63 specimens under quasi-static monotonic and reversed cyclic loading, evaluating load–displacement and hysteretic curves to determine connection yield load, yield slip, capacity, stiffness, and ductility. However, the study did not assess overstrength or employ a more advanced connection model, such as a finite-element model. Hossain et al. (2019) [41] focused on determining group-effect reduction factors for strength, stiffness, and ductility of shear connections with STS in CLT under monotonic and cyclic loading. They conducted 175 monotonic and cyclic tests, varying the number of STS in one row between 2 and 32. However, none of the aforementioned papers attempted to assess the uncertainty propagation from model parameters to the capacity estimate for CLT-to-CLT screwed connections

For the first time, this paper estimates the overstrength of CLT-to-CLT connections with inclined screws. The paper discusses the limits of the equation in Eq. (1), by providing a probabilistic formulation of the equation by [11], which can be used for estimating the overstrength level when different reliability thresholds are considered. Additionally, the paper gives an insight into the role of epistemic and aleatoric uncertainty in estimating overstrength. To the authors' knowledge, no paper attempted to isolate the contributions of the two uncertainty sources to overstrength for any timber connections. The main reason for this investigation is the limits of typical experimental campaigns for estimating the overstrength of CLT connections, generally based on a limited number of test repetitions for each configuration.

While the experimental campaigns encompass a variety of test configurations, the number of test repetitions is deliberately kept to a minimum to assess a reasonable coefficient of variation. This practice is commonly adopted to balance the need for sufficient data and cost considerations. As a result, the number of test repetitions is not determined based on stabilization criteria, such as reaching a threshold coefficient of variation. Instead, it is a predetermined number decided before conducting the tests, and it may not be sufficient for a comprehensive characterization of the experimental scatter. While it is impractical to repeat the same configuration until the coefficient of variation stabilizes, it is possible to simulate the range of test outcomes using appropriate mechanical models that account for parameter uncertainty and propagate it to the final capacity estimation. It is important to note that the considered test repetitions generally exhibit limited variability in geometric and mechanical parameters due to the use of the same wood and screw stock, as well as the consistent assembly of specimens by the same person in a controlled testing laboratory environment, which is typically more controlled than a construction site. One critical aspect is the potential variation in screw angles, which may deviate from the precise 45° angle. In this paper, the authors conducted push-out tests by varying both the CLT panel types and the types of screws. The additional sources of uncertainty were then incorporated into the two capacity models, namely the analytical and finite element-based models. Future research efforts will focus on integrating other uncertainty sources into the experimental campaign.

Therefore, it is essential to isolate the role of epistemic and aleatoric uncertainty in a numerical-based assessment of overstrength, where the model parameters are random variables representative of the actual connection uncertainty.

The authors present a method for estimating a model-driven overstrength factor, more representative of the as-built connection. This estimate is corrected to remove the epistemic bias using the experimental results. Two mechanical models are compared to predict the overstrength in CLT-to-CLT screw connections: the classical capacity model in EC5 and a nonlinear finite element model developed in Abaqus. In the first step, the capacity of the connection is simulated by randomly sampling the model parameters from given probability distributions (PDF) representative of the experimental tests. The results of this analysis provide the epistemic correction, which is used to evaluate the overstrength factor assuming more realistic PDFs for the model parameters.

2. Problem formulation

This section will first provide a generalized expression for the γ_{Rd} proposed by [11]. Then, the authors will present the method for assessing the two sources of uncertainties, epistemic and aleatoric to overstrength.

2.1. Probabilistic interpretation of the formulation by Jorissen and Fragiacomo

The classical definition of overstrength is based on the following limit state function [12,14]:

$$\underbrace{\gamma_{Rd} R_{\mathrm{dct,an},d}}_{\text{Demand}} - \underbrace{R_{\mathrm{brt}}}_{\text{Capacity}} \leq 0 \tag{2}$$

where R_{brt} is the load-carrying capacity of the non-ductile element described by a suitable probability distribution, and $R_{\mathrm{dct,an},d}$ is the design load-carrying capacity of the ductile element estimated from an analytical capacity model. The inequality in Eq. (2) conveys the following design requirement: the actual resistance of the ductile element, whose upper bound is ($\gamma_{Rd} R_{\mathrm{dct,an},k}$), cannot exceed the brittle resistance. Otherwise, the brittle mechanism occurs before the ductile one. γ_{Rd} is an amplification factor that maximizes the predicted ductile element's resistance to quantify the possible overstrength due to all uncertainties involved in the capacity equation.

According to Eq. (2), the overstrength factor originates from a limit state function. Adopting the classical nomenclature of structural reliability, the resistance of the brittle element represents capacity. At the same time, the demand is expressed by the characteristic resistance of the ductile element multiplied by γ_{Rd}. The estimation of γ_{Rd} demands the assessment of the ductile and brittle mechanisms and their uncertainties. γ_{Rd} can be estimated by setting a given reliability threshold, depending on the limit state under consideration, as follows:

$$\text{Find } \gamma_{Rd} : P(\gamma_{Rd} \cdot R_{\text{dct,an},k} - R_{\text{brt}} \leq 0) = \hat{p}_f \tag{3}$$

where $\hat{p}_f$ is a failure probability threshold. According to the definition in Eq. (2), γ_{Rd} is a relational property between failure mechanisms depending on the accepted reliability target.

Despite the theoretical validity, Eq. (2) is challenging to use in many situations. The main difficulty is the relational definition, brittle vs ductile, which is difficult to compute directly from experimental tests where a specific failure mechanism is observed.

Therefore, Jorissen and Fragiacomo [11] provided a different interpretation to Eq. (2). They did not interpret γ_{Rd} as a sort of power ratio between failure mechanisms with different ductility. It is indeed a property of the sole ductile mechanisms. Accordingly, the limit state function in Eq. (2) can be re-formulated as follows:

$$\underbrace{\gamma_{Rd} R_{\text{dct,an},d}}_{\text{Demand}} - \underbrace{R_{\text{dct,exp}}}_{\text{Capacity}} \leq 0 \tag{4}$$

Following the classical interpretation of structural reliability, the demand is the left term, which is the $\gamma_{Rd} R_{\text{dct,an},d}$, where $R_{\text{dct,an},d}$ is the design value of the resistance of the ductile element. The capacity is represented by the capacity of the ductile element($R_{\text{ductile,exp}}$), described by a suitable probability distribution.

The estimation of the overstrength using Eq. (4) provides a sort of upper bound to γ_{Rd}, if the following holds: $R_{\text{dct,exp}} < R_{\text{brt,exp}}$.

The definition in Eq. (4) modifies the idea behind Eq. (6). The overstrength factor becomes a property of the ductile mechanism, expressing the variability of its value related to epistemic and aleatoric uncertainties. Based on Eq. (4), γ_{Rd} can be estimated as follows:

$$\text{Find } \gamma_{Rd} : P(\gamma_{Rd} R_{\text{dct,an},d} - R_{\text{dct,exp}} \leq 0) = \hat{p}_f \tag{5}$$

where $R_{\text{dct,an},d}$ is deterministic and $R_{\text{dct,exp}}$ is described by a given probability density function.

If the resistance of the ductile element, generally obtained from experimental tests, is approximated by a normal distribution,

$$R_{\text{dct,exp}} \sim \mathcal{N}[\mu = R_{\text{dct,exp},m}, \sigma = \text{Std.Dev.}(R_{\text{dct,exp}})] \tag{6}$$

where $R_{\text{dct,exp},m}$ and Std.Dev.($R_{\text{dct,exp}}$) are the mean value (μ) and the standard deviation (σ) of a Normal distribution ($\mathcal{N}$), then, the limit state function in Eq. (4) can be written as:

$$P(\gamma_{Rd} R_{\text{dct,an},d} - R_{\text{dct,exp}} \leq 0) \sim \mathcal{N}[\mu = (\gamma_{Rd} R_{\text{dct,an},d} - R_{\text{dct,exp},m}), \quad \sigma = \text{Std.Dev.}(R_{\text{dct,exp}})] \tag{7}$$

The reliability index (β) has the following closed-formed expression for Normal distributions

$$\mu = \beta\sigma \rightarrow \gamma_{Rd} R_{\text{dct,an},d} - R_{\text{dct,exp},m} = \beta\sigma \tag{8}$$

$$\gamma_{Rd} = \frac{R_{\text{dct,exp},m} + \beta\sigma}{R_{\text{dct,an},d}} \tag{9}$$

If the reliability target is $\beta = 1.64$, the formulation by Jorissen and Fragiacomo can be obtained since $R_{\text{dct,exp},k} = R_{\text{dct},exp,m} + 1.64\sigma$. Similarly, also the definition from the Building Research Association of New Zealand (BRANZ) [42] can be obtained

$$\gamma_{\text{Rd}} = \frac{R_{\text{dct,exp},0.95}\left(1 + \frac{2.7\theta}{\sqrt{n}}\right)}{R_{\text{dct,exp},0.05}\left(1 - \frac{2.7\theta}{\sqrt{n}}\right)} \tag{10}$$

where θ is the variation coefficient of test results; n is the number of tests.

The above algebraic passages highlight the probabilistic interpretation of Eq. (1), which can also be easily computed if higher reliability targets are required. If fact, $\beta = 1.64$ is a threshold corresponding to a serviceability limit state. If a higher reliability class is considered, a higher β should be used in Eq. (9).

In this paper, the authors will estimate the overstrength of CLT-to-CLT screwed connections addressing the role of β in the overstrength calculation. This calculation will allow comparing the estimations of γ_{Rd} from Eq. (1) and those obtained with higher βs.

Specifically, the overstrength factor can be factorized as follows [43]:

$$\gamma_{Rd} = \gamma^*_{Rd} \cdot \gamma_M \tag{11}$$

where the partial overstrength factor (γ^*_{Rd}) is:

$$\gamma^*_{Rd} = \frac{R_{\text{dct,exp},m} + \beta\sigma}{R_{\text{dct,an},k}} \tag{12}$$

Eq. (12) allows calculating the overstrength without the contribution of the partial safety factor, which varies from code to code. Eq. (12) provides a straightforward approach for calculating the overstrength from experimental tests, considering a variable reliability target depending on the chosen limit state. This will allow quantifying the difference between the predictions following Eq. (12) with typical β values considered at the ultimate limit state (3.8, e.g.) and Eq. (1).

2.2. Estimation of the aleatoric and epistemic uncertainties in overstrength

In the classical definition of overstrength in Eq. (1), the numerator is experimental-based and the denominator is obtained from the capacity model. However, the overstrength factor estimated from Eq. (1) might not represent the actual scatter of the capacity values. A limited number of experiments are generally carried out using the same wood and screw stocks, characterized by limited variabilities. Additionally, in real cases, additional random variables might increase the scatter of the capacity, like the screw inclination. In the working site, the workers do not always use a template to obtain a specific inclination of the screw. Therefore, the overstrength factor from Eq. (1) might be underestimated.

Parallelly, suppose the overstrength is entirely predicted from a suitable mechanical by propagating the uncertainties from the model parameters to the capacity estimate. In that case, the estimation could be biased for two main reasons:

- The existence of a possible bias (μ_{epi}) between the expected values of the experimental (E($R_{\text{dct,exp}}$)) and model capacities (E($R_{\text{dct,mod}}$)). This is the epistemic bias of the mechanical model, which can be easily estimated from the difference between E($R_{\text{dct,exp}}$) and E($R_{\text{dct,mod}}$).
- The standard deviation σ_{mod} predicted by the model might be over or underestimated compared to the experimental one. Therefore, it is essential to remove the contribution of epistemic uncertainty to the model estimate of the standard deviation. The experimental standard deviation, in Eq. (12), is only representative of the aleatoric uncertainty due to the intrinsic scatter of the material properties and connection details.

Therefore, a model-driven overstrength assessment requires correcting the total model uncertainty from the contribution of the epistemic one. The problem can be formalized as follows. The capacity predicted from a model can be written as:

$$R_{\text{dct,mod}}(\boldsymbol{x}, \boldsymbol{\Theta}) = \text{E}(R_{\text{dct,mod}}) + \mathcal{E}_{\text{mod}} \tag{13}$$

where $R_{\text{dct,mod}}(\boldsymbol{x}, \boldsymbol{\Theta})$ is the capacity of the ductile mechanisms estimated from a mechanical model, $\boldsymbol{x}$ are the model parameters and $\boldsymbol{\Theta}$

express their related uncertainty; E is the expected value operator, and $\mathcal{E}_{\text{mod}}$ is the difference between the predicted and the expected value of the capacity.

The total error ($\mathcal{E}_{\text{mod}}$) can be viewed as the symbolic summation between the epistemic and aleatoric uncertainties:

$$\mathcal{E}_{\text{mod}} = \mathcal{E}_{\text{epi}} + \mathcal{E}_{\text{al}} \tag{14}$$

where $\mathcal{E}_{\text{epi}}$ is the epistemic error and $\mathcal{E}_{\text{al}}$ the aleatoric error. The aleatoric uncertainty, also known as stochastic uncertainty, is representative of unknowns that differ each time we repeat the same experiment. In this circumstance, it expresses the intrinsic scatter of the material and connection parameters. In CLT-to-CLT screw connections, the parameters mainly affecting the model error are the wood density (ρ), the friction coefficient (m), the yielding strength of steel (f_y) and the screw inclination (α). The uncertainty of the wood density indirectly affects the stiffness and strength parameters of the connection, as proven by consolidated empirical regressions between them and the wood density [44]. Epistemic uncertainty is also known as systematic uncertainty and is due to phenomena one could, in principle, know but does not in practice. In this case, this uncertainty depends on the limits of the capacity model, which neglects specific effects. It is impossible to isolate the contributions of the two sources of uncertainties to the total one in Eq. (14), where the two are summed up.

Additionally, while it is possible to estimate the probability distribution of the numerical capacity from a large number of numerical simulations, it is not possible to accurately estimate the probability distribution of the experimental capacity. In most circumstances, a maximum of five repetitions of the same experimental configuration is carried out. Therefore, it is generally assumed that the probability distribution of the experimental values is normal or lognormal. For homogeneity, the normality hypothesis can also be assumed for the model uncertainty estimated from the model through Montecarlo simulations. Therefore, the error function can be approximated as follows, if the normality assumption holds:

$$\mathcal{E}_{\text{mod}} \sim \mathcal{N}(\mu_{\text{epi}}, \sigma_{\text{mod}}); \text{ where } \mu_{\text{epi}} = \text{E}(R_{\text{dct,exp}}) - \text{E}(R_{\text{dct,mod}}) \quad \sigma^2_{\text{mod}}(\boldsymbol{x}, \boldsymbol{\Theta}) = \sigma^2_{\text{al}} + \sigma^2_{\text{epi}} \tag{15}$$

where $\mathcal{N}$ is a Normal distribution, μ_{epi} is the epistemic bias, σ^2_{mod}, σ^2_{epi} and σ^2_{al} are the model, epistemic and aleatoric standard deviations, respectively. The epistemic and aleatoric error functions can be written as:

$$\mathcal{E}_{\text{epi}} \sim \mathcal{N}(\mu_{\text{epi}}, \sigma_{\text{epi}}); \quad \mathcal{E}_{\text{al}} \sim \mathcal{N}(0, \sigma_{\text{al}}); \tag{16}$$

It can be assumed that the ratio between the aleatoric and model standard deviation is constant and independent of the value of the model error.

$$k = \frac{\sigma_{\text{al}}}{\sigma_{\text{mod}}(\boldsymbol{x}, \boldsymbol{\Theta})} = \frac{\sigma_{\text{exp}}}{\sigma_{\text{mod}}(\boldsymbol{x}_{\text{exp}}, \boldsymbol{\Theta}_{\text{exp}})} \tag{17}$$

where σ_{exp} is the standard deviation obtained from the experimental tests and $(\boldsymbol{x}_{\text{exp}}, \boldsymbol{\Theta}_{\text{exp}})$ are the model parameters representative of the experimental tests. Therefore, it is possible to correct the model standard deviation from the epistemic contribution if k is known. Specifically, as shown in Eq. (17), if the model standard deviation is predicted with model parameters representative of the experimental tests ($\{\boldsymbol{x}, \boldsymbol{\Theta}\} = \{\boldsymbol{x}_{\text{exp}}, \boldsymbol{\Theta}_{\text{exp}}\}$), then σ_{exp} can be set equal σ_{al}.

$$\sigma^2_{\text{mod}}(\boldsymbol{x}_{\text{exp}}, \boldsymbol{\Theta}_{\text{exp}}) = \sigma^2_{\text{al}} + \sigma^2_{\text{epi}} = \sigma^2_{\text{exp}} + \sigma^2_{\text{epi}} \tag{18}$$

Accordingly, it is possible to assess the ratio between the aleatoric and model standard deviation (k) from Eq. (17), where the numerator is the experimental standard deviation, and the denominator is the model standard deviation obtained by propagating the parameter uncertainty ($\boldsymbol{\Theta} = \boldsymbol{\Theta}_{\text{exp}}$), representative of the experiments, through the capacity model.

Algorithm 1 Pseudo-code

Define $\boldsymbol{x}_{\text{exp}} = \{f_{y,m,\text{exp}}, \rho_{\text{exp}}, m_{m,\text{exp}}, \alpha_{m,\text{exp}}\}$ and $\boldsymbol{\Theta}_{\text{exp}} = \{\text{CoV}_{fy,\text{exp}}, \text{CoV}_{\rho,\text{exp}}, \text{CoV}_{m,\text{exp}}, \text{CoV}_{\alpha,\text{exp}}\}$ ▷ Uncertainty of input parameters based on experimental tests
while $\text{CoV}(R_{\text{dct,mod}}(1:n) < 0.01)$ **do**
  Quasi-MC Halton sampling of parameters' sets $\boldsymbol{x} = \{f_y, \rho, \mu\}$
  Simulate $R_{\text{dct,mod}}$ given the sampled parameters ($\boldsymbol{x}$) ▷ Capacity estimate from the model
  $\boldsymbol{R}_{\text{dct,mod}} = R_{\text{dct,mod}}(1:n)$ ▷ Allocate the simulated values in a vector of size n
end while
$\sigma_{\text{mod}}(\boldsymbol{x}_{\text{exp}}, \boldsymbol{\Theta}_{\text{exp}}) = \text{Std.Dev.}[\boldsymbol{R}_{\text{dct,mod}}(\boldsymbol{x}_{\text{exp}}, \boldsymbol{\Theta}_{\text{exp}})]$
$\sigma_{\text{exp}} = \text{Std.Dev.}(R_{\text{dct,exp}})$
$\mu_{\text{epi}} = \text{E}(R_{\text{dct,exp}}) - \text{E}(R_{\text{dct,mod}})$; ▷ Computation of the epistemic bias

$k = \frac{\sigma_{\text{exp}}}{\sigma_{\text{mod}}}(\boldsymbol{x}_{\text{exp}}, \boldsymbol{\Theta}_{\text{exp}})$; ▷ Computation of the epistemic correction factor

Define $\boldsymbol{x} = \{f_y, \rho, m\}$ and $\boldsymbol{\Theta} = \{\text{CoV}_{fy}, \text{CoV}_{\rho}, \text{CoV}_{m}\}$ ▷ Uncertainty of input parameters based on scientific literature
while $\text{CoV}(R_{\text{dct,mod}}(1:n) < 0.01)$ **do**
  Quasi-MC Halton sampling of parameters' sets $\boldsymbol{x} = \{f_y, \rho, m\}$
  Simulate $R_{\text{dct,num}}$ given the sampled parameters (Θ)
  $\boldsymbol{R}_{\text{dct,mod}} = R_{\text{dct,mod}}(1:n)$
end while
$\sigma_{\text{mod}}(\boldsymbol{x}, \boldsymbol{\Theta}) = \text{Std.Dev.}(R_{\text{dct,mod}}(1:n))(\boldsymbol{x}, \boldsymbol{\Theta})$
Compute $\gamma_{Rd,\text{mod}}$ from Eq.(19).

Then, the model-driven partial overstrength factor ($\gamma^*_{Rd,\text{mod}}$) using different values for $\{\boldsymbol{x}, \boldsymbol{\Theta}\}$, is:

$$\gamma^*_{Rd,\text{mod}} = \frac{\text{E}[R_{\text{dct,mod}}(\boldsymbol{x}, \boldsymbol{\Theta})] + \mu_{\text{epi}}(\boldsymbol{x}, \boldsymbol{\Theta}) + k \cdot \beta \cdot \sigma_{\text{mod}}(\boldsymbol{x}, \boldsymbol{\Theta})}{R_{\text{dct,an},k}} \tag{19}$$

The improvement of Eq. (19) compared to Eq. (12) are the followings:

- The overstrength factor is representative of the actual scatter of the connection parameters observed in real-case scenarios. In general, it happens that $\boldsymbol{\Theta} > \boldsymbol{\Theta}_{\text{exp}}$;
- The numerator only includes the contribution of the aleatoric uncertainty, as occurring in Eq. (12), due to an epistemic correction factor (k) defined in Eq. (17) calibrated on the experimental tests.
- The reliability target (β) is explicited.

Additionally, this expression can predict overstrength ratios for different parameter uncertainties. It must be remarked, that γ^*_{Rd} from Eq. (12) equals $\gamma^*_{Rd,\text{mod}}$ if the model parameters represent the experiential test, i.e. $\{\boldsymbol{x}, \boldsymbol{\Theta}\} = \{\boldsymbol{x}_{\text{exp}}, \boldsymbol{\Theta}_{\text{exp}}\}$

$$\gamma^*_{Rd,\text{mod}} = \gamma^*_{Rd,\text{exp}} \text{ if } \{\boldsymbol{x}, \boldsymbol{\Theta}\} = \{\boldsymbol{x}_{\text{exp}}, \boldsymbol{\Theta}_{\text{exp}}\}. \tag{20}$$

Algorithm 1 provides the pseudocode corresponding to the calculation of the $\gamma^*_{Rd,\text{num}}$ according to Eq. (19).

The calculation of the overstrength requires two Montecarlo simulations assessing $\sigma_{\text{mod}}(\boldsymbol{x}_{\text{exp}}, \boldsymbol{\Theta}_{\text{exp}})$ and $\sigma_{\text{mod}}(\boldsymbol{x}, \boldsymbol{\Theta})$ respectively. The first leads to the estimation of k, according to Eq. (17) the second to $\gamma^*_{Rd,\text{num}}$ according to Eq. (19). In the first MCS, the authors assume that f_y, m, ρ and α are normally distributed, with the parameters of the distribution obtained from the tests on the material used for the specimen preparation in the experimental campaign. In the second MCS, the authors assume the same parameters as normally distributed, with the distribution parameters obtained from the scientific literature. The two MCS are described in the pseudocode by a while loop which stops if the convergence criterion is met. The convergence criterion is the limit value to the coefficient of variation of the model capacity.

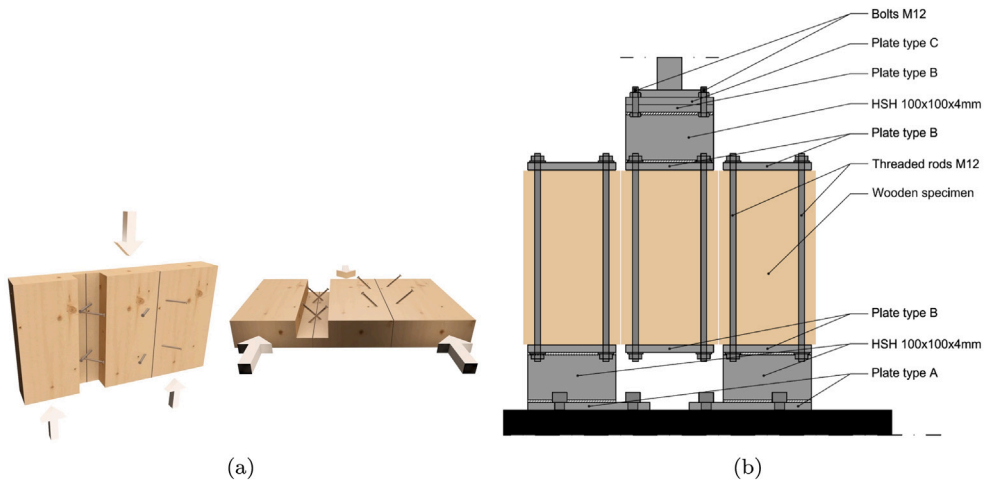

Fig. 2. (a) Front 3D and exploded views of the considered connection typology; (b) Experimental setup.

The parameters of the distribution are sampled with a Halton sampling scheme. The other passages in Algorithm 1 are straightforward algebraic passages, that lead to the estimate of the Eq. (19).

The predictive model of the capacity can be either numerical or analytical. In this paper, the authors will compare the predictions using the analytical capacity model in Eq. (21) and a more complex nonlinear FE model. The latter might better reproduce the complex nonlinear mechanical response of the connection and, accordingly, more faithfully reproduce the uncertainty propagation from the material parameters to the capacity.

3. Experimental tests

The authors carried out push-out tests to evaluate the shear resistance of CLT-to-CLT screw connections. The connection between two adjacent parallel panels follows the configuration (c) in Fig. 1. This solution avoids the cuts needed for lap or spline joints, which are easily made in the production line but are challenging to obtain on-site.

Fig. 2 shows this connection's front and exploded views. Although the screws are inserted with a 45° angle, such an angle does not influence the connection resistance since the force direction is orthogonal to the screws. The experimental configuration consists of three specimens with 350 mm × 200 mm size, jointed by screws along their long narrow side, as shown in Fig. 2(b). This configuration grants a symmetrical application of the vertical load. The authors tested six different configurations, each one with five repetitions. Therefore, the total number of tests is $6 \times 5 = 30$.

The differences between the configurations stand in the (i) CLT panel and (ii) the types of screws. Specifically, the authors tested three CLT panel layups with thicknesses equal to 80 mm (30 + 20 + 30), 100 (20 + 20 + 20 + 20 + 20) and 120 mm (30 + 20 + 20 + 20 + 30), respectively.

Table 1 shows the details of the screws. There are two main types, the fully-threaded VGZ screws produced by Rothoblaas and the partially-threaded WT screws made by SFS. The latter has two different and separated threads along their length; see Fig. 3(b).

The maximum length for the fasteners was calculated by multiplying the panel thickness by the square root of 2. The authors selected the commercial screws with the size closest to the initial estimate. The diameter of the screws ranged between 6.2 to 9 mm, with a length between 100 and 160 mm. The screws are inserted, without predrilling, with their axes perpendicular to the grain direction of the outer layer and at 45° to the plane of the panels. An accurate insertion angle is obtained through a steel template shown in Fig. 3(c). It consists of a steel plate welded on a directing tube.

Table 1
Details of the tested configurations.

Label	Screw type	Diameter [mm]	Panel thickness [mm]	Screw length [mm]
V7-80	VGZ Rothoblaas	7	80	100
V7-100	VGZ Rothoblaas	7	100	140
V7-120	VGZ Rothoblaas	7	120	140
V9-120	VGZ Rothoblaas	9	120	160
W6-120	WT SFS	6.5	120	160
W8-120	WT SFS	8.2	120	160

The identifying label of the specimens in Table 1 has been chosen as follows: the first letter refers to the screw type, which is V for VGZ screws (Rothoblaas) and W for WT screws (SFS). The following number indicates the nominal diameter of the screw (neglecting tenths of a millimetre). The following number indicates the thickness of the CLT specimen, while the last one, ranging from 1 to 5, is the test repetition. All specimens were tested with an Instron SATEC series 8800 model 300 KN static hydraulic universal testing system in Fig. 4. The machine has a maximum capacity of 300 kN.

The monotonic tests were carried out according to EN 26891:199145. The loading protocol consists in an initial cycle that settles the specimen and the remaining to reach the ultimate load. In the first cycle, the load is applied up to 40% of the estimated capacity, which is held for 30 s. Then the load is decreased to 10% of the estimated capacity and kept for 30 s more. If the load is below 70% of the estimated capacity, the load is applied at a constant rate, consisting of an increase of 0.2 of the estimated capacity per minute. Beyond 70%, the load is applied at constant displacement speed so that the failure or displacement of 15 mm is reached within 15 min. The speed was hence decided to achieve the goal displacement of 15 mm within the prescribed time. The specimens, however, showed a deformation capacity much higher than 15 mm, and it was decided to continue the testing until a drop of 20% of the measured force.

3.1. Capacity prediction

The shear capacity of the connection is predicted by Johansen's equations implemented in the current EC5. The minimum distances indicated in EC5 refer to solid or glue-laminated timber and are generally

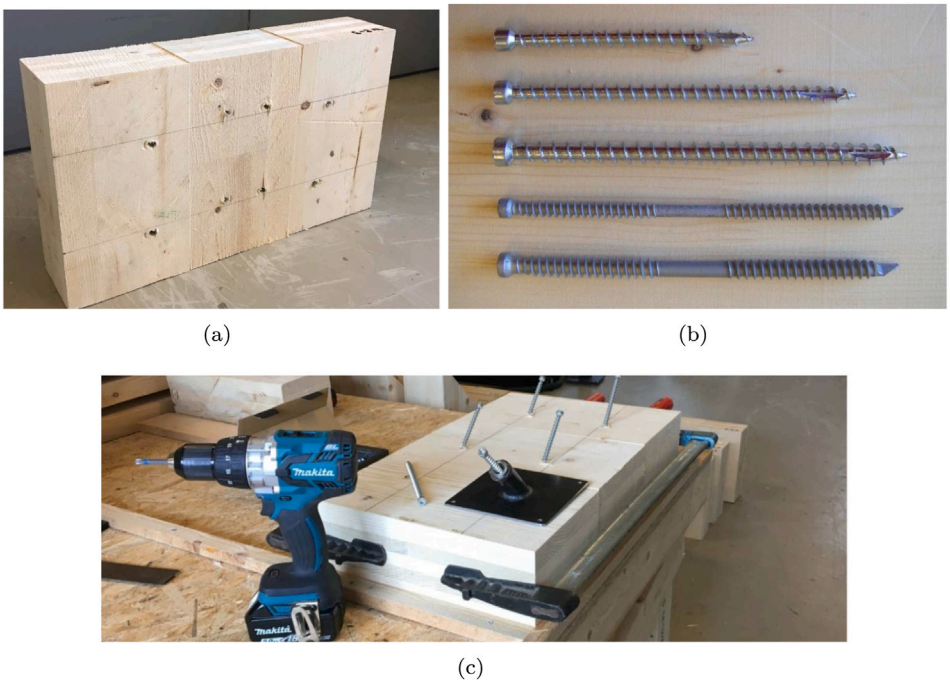

Fig. 3. (a) tested configuration; (b) Views of the screws; (c) detail of the steel template used for the screw insertion with a 45° angle.

Fig. 4. View of the experimental test.

Table 2
Minimum distances adopted from the screws inserted in CLT panels.

Screw	d	a_1	a_{3c}	a_{3t}
VGZ7	7	28	42	42
VGZ9	9	36	54	54
WT-T-6.5	6.5	26	39	39
WT-T-8.2	8.2	32.8	49.2	49.2

not valid for CLT. Therefore, the minimum distances for the screws inside CLT were chosen after [45], as reported in Table 2. The same values can be found in the ETA document for the Rothoblaas VGZ screws. The distance between the screws and the edges of the panel is 100 mm, which is higher than the minimum values in Table 2. The minimum distance between two crossing screws is set as 20 mm.

The shear capacity of the connection is the minimum between the values associated with six different failure mechanisms, labelled from (a) to (f) and illustrated in Fig. 5 [46]:

$$F_{v,Rk} = \begin{cases} f_{h,1,k} \cdot t_1 \cdot d & (a) \\ f_{h,2,k} \cdot t_2 \cdot d & (b) \\ \frac{f_{h,1,k} t_1 d}{1+\gamma} \left\{ \sqrt{2 + 2\gamma^2 \left[1 + \frac{t_2}{t_1} + \left(\frac{t_2}{t_1}^2 \right) \right] + \gamma^3 \left(\frac{t_2}{t_1} \right)^2} - \gamma \left(1 + \frac{t_2}{t_1} \right) \right\} + \frac{F_{ax,k}}{4} & (c) \\ \frac{f_{h,1,k} t_1 d}{2+\gamma} \left[\sqrt{2\gamma(1+\gamma) + \frac{4\gamma(2+\gamma) M_{y,Rk}}{f_{h,1,k}} \cdot d \cdot t_1^2} - \gamma \right] + \frac{F_{ax,Rk}}{4} & (d) \\ \frac{f_{h,1,k} t_2 d}{2+\gamma} \left[\sqrt{2\gamma(1+\gamma) + \frac{4\gamma(2+\gamma) M_{y,Rk}}{f_{h,1,k}} \cdot d \cdot t_2^2} - \gamma \right] + \frac{F_{ax,Rk}}{4} & (e) \\ \sqrt{\frac{2\gamma}{1+\gamma}} \cdot \sqrt{2 M_{y,Rk} \cdot f_{h,1,k} d} + \frac{F_{ax,Rk}}{4} & (f) \end{cases} \quad (21)$$

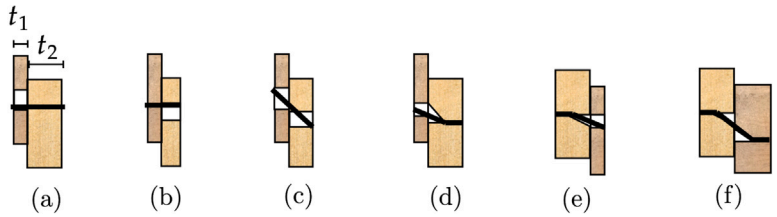

Fig. 5. Failure modes according to the Johansen theory, each one described analytically in Eq. (21).

where $F_{v,Rk}$ is the characteristic load-bearing capacity of a single fastener per shear plane; $M_{y,Rk}$ is the characteristic yielding moment of the fastener, d is the fastener diameter; $f_{h,1,k}$ and $f_{h,2,k}$ are the characteristic embedding strengths of the two connected timber elements; t_1 and t_2 are the penetration lengths of the screw in each element, γ is the ratio between $f_{h,2,k}$ and $f_{h,1,k}$ and, finally, $F_{ax,Rk}$ is the characteristic withdrawal strength. In this case, $f_{h,1,k}$ and $f_{h,1,k}$ are equal, and γ is equal to 1. Regarding t_1 and t_2, the screws have been inserted so that the middle of their length is exactly within the shear plane. This leads to t_1 being equal to t_2.

The characteristic embedding strength ($f_{h,1,k}$) for fully-threaded self-tapping screws can be calculated according to the formula proposed by [47]:

$$f_{h,k} = 0.019 \cdot \rho_{B,k}^{1.24} \cdot d^{-0.3} \tag{22}$$

where d is the nominal diameter of the screws in mm and $\rho_{B,k}$ is the characteristic bulk density of the material in kg/m^3. According to EN 33841, the characteristic density is $\rho_{B,k}$ = 350 kg/m^3. It is worth noting that in the Johansen model a constant embedment strength is assumed in each member. Consequently, the model cannot account for the actual panel layup. An empirical model exists to predict an equivalent embedment strength [45]; however, in the following, the authors use the models recommended by the EC5. The characteristic withdrawal resistance of fully-threaded self-tapping screws inserted in the lateral surface of the panel can be calculated according to [45]:

$$F_{ax,k} = \frac{31 \cdot d^{0.8} \cdot l_{ef}^{0.9}}{1.5 \cos^2 \alpha + \sin^2 \alpha} \tag{23}$$

where l_{ef} is the effective screw penetration depth in mm, and ϵ is the screw angle in radians to the grain in the surface layer. In this case, the values of l_{ef} employed for VGZ screws are calculated as half of the length of the threaded part of the screw minus 5 mm, which is the installation tolerance. For the WT screws, the values of l_{ef} employed should consider the non-threaded portion of the screw between the two threaded ones. Therefore, the minimum effective threaded length of the screw is derived from the ETA document without considering any tolerance for the installation. Finally, the value of α is always 90° since the screws are inserted in the lateral surface of the panel perpendicularly to the direction of the grain of the outer layer.

The characteristic yielding moment of a cylindrical fastener according to the EC5 is calculated as:

$$M_{y,Rk} = 0.3 \cdot f_{y,k} \cdot d_{ef}^{2.6} \tag{24}$$

where $f_{u,k}$ is the characteristic tensile strength of the steel in N/mm^2 and d_{ef} is the effective diameter of the fastener in mm. For a fully-threaded screw, the effective diameter is 1.1 times the core diameter. Table 3 collects the values of the embedment strength, axial capacity and yielding moment of the considered fasteners.

It is worth noting that the values for $M_{y,Rk}$ proposed and certified by producers are lower than those calculated according to the standards. Ultimately the more conservative values of the ETA document were adopted.

Failure mode f) provides the lowest resistance for all the considered configurations. Two plastic hinges in the fastener characterize this failure mode. This failure mode exhibits the most ductile and dissipative behaviour since it fully exploits the ductility of steel. Table 4 collects the predicted values of the capacity of the single fastener and the entire connection according to EC5.

3.2. Results

A visual inspection of the tested specimen provides a preliminary insight. No brittle failures occurred during the testing. Moreover, each sample reached large deformations before failure, showing a manifest ductile behaviour. Disassembling the specimen allowed a closer inspection that confirmed the formation of two plastic hinges in the fasteners, as proven in Fig. 6. The screws formed two visible plastic hinges that confirmed the failure mode predicted by Johansen's theory in Eq. (21). All the tested samples reached, in fact, an ultimate displacement greater than 19 mm, and on average equal to 37 mm.

Fig. 7 shows the experimental force–displacement curves for each tested configuration, each one with five repetitions. Table 10 resumes the following mechanical properties estimated from each curve: The elastic ($k_{el,exp}$ according to EN125129) and plastic stiffness ($k_{pl,exp}$ according to the Y&K method [1]); The yielding ($F_{y,exp}$), maximum ($F_{max,exp}$) and ultimate ($F_{u,exp}$) force values; The yielding ($v_{y,exp}$) and ultimate (v_u) displacements and the ductility ratio (D_{exp}). The detailed definition of each parameter is given in the initial list of symbols and notation (see Table 5).

It must be remarked, that all specimens exhibited high ductility values, ranging from a minimum mean value of 11.65 obtained from the V9 configuration to the maximum mean value of 30.18 obtained from the W8 configuration. This fact confirms the reason why the vertical connection between wall elements for CLT buildings is acknowledged as the most ductile one and is devoted to dissipative behaviour for buildings designed in high ductility class in the draft proposal for the new section 8 of Eurocode 8.

Once the necessary data from each sample was extrapolated, mean values, 5th percentile, 95th percentile and standard deviations were derived following EN1435831. The characteristic value is obtained as follows:

$$F_{\mathrm{dct,exp},k} = F_{\mathrm{dct,exp},m} - k_s \sigma_{\mathrm{exp}} \tag{25}$$

where k_s = 2.64 for five specimens according to EN:14358:2016.

Table 6 compares all the relevant quantities necessary to evaluate the overstrength ratios.

The first row in Table 6 shows the characteristic resistance predicted according to Eq. (21). The second and third rows show the experimental mean capacity and the corresponding standard deviation. It is interesting to observe that the predicted CoV 0.2, is lower than the experimental one, which is 0.29. The standard deviation approximately ranges between 2 and 3, with a maximum of nearly 6 for V9. The third block row of Table 6 reports the mechanical parameters used for estimating the overstrength ratio. The γ_{sc}, representative of the scatter of the experimental data ranges between 1.30 and 1.50, meaning that 95% percentile of the capacity can be between 1.3 and 1.5 the characteristic value. The γ_{an}, representative of the analytical model error, exhibits a larger variability, from 1.1 up to 1.6. The analytical model significantly underestimates the characteristic capacity by approximately 40%. The

Table 3
Table collecting the values of the embedment strength, axial capacity and yielding moment of the considered fasteners.

Screw	d [mm]	l_{ef} [mm]	$f_{h,k}$ [Mpa]	$F_{ax,k,s}$ [kN]	d_{core} [mm]	$f_{u,k}$ [MPa]	$M_{y,Rk}$ [kNmm]	$M_{y,Rk,\mathrm{ETA}}$ [kN mm]
VGZ 7 × 100	7	40	15.1	5.1	4.6	1000	20.3	14.2
VGZ 7 × 140	7	60	15.1	5.9	4.6	1000	20.3	14.2
VGZ 9 × 160	9	70	14.0	8.2	5.9	1000	38.8	27.2
WT 6.5 × 160	6.5	65	15.5	5.9	4.0	990	14.0	12.7
WT 8.2 × 160	8.2	65	14.4	7.1	5.4	870	26.8	19.5

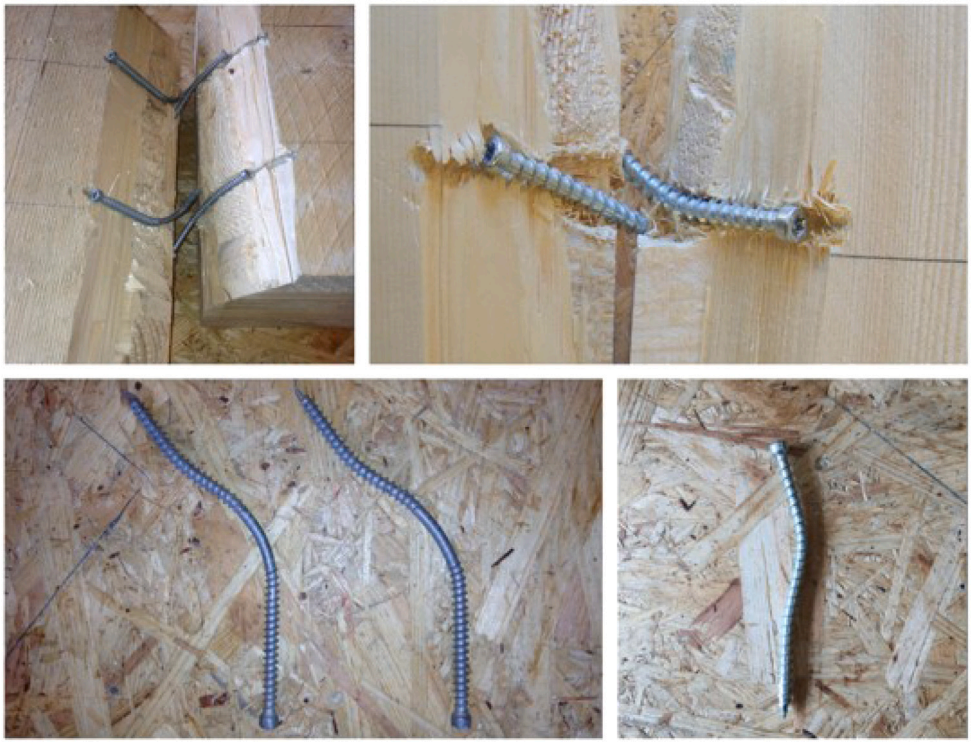

Fig. 6. Failure mode of experimental tests.

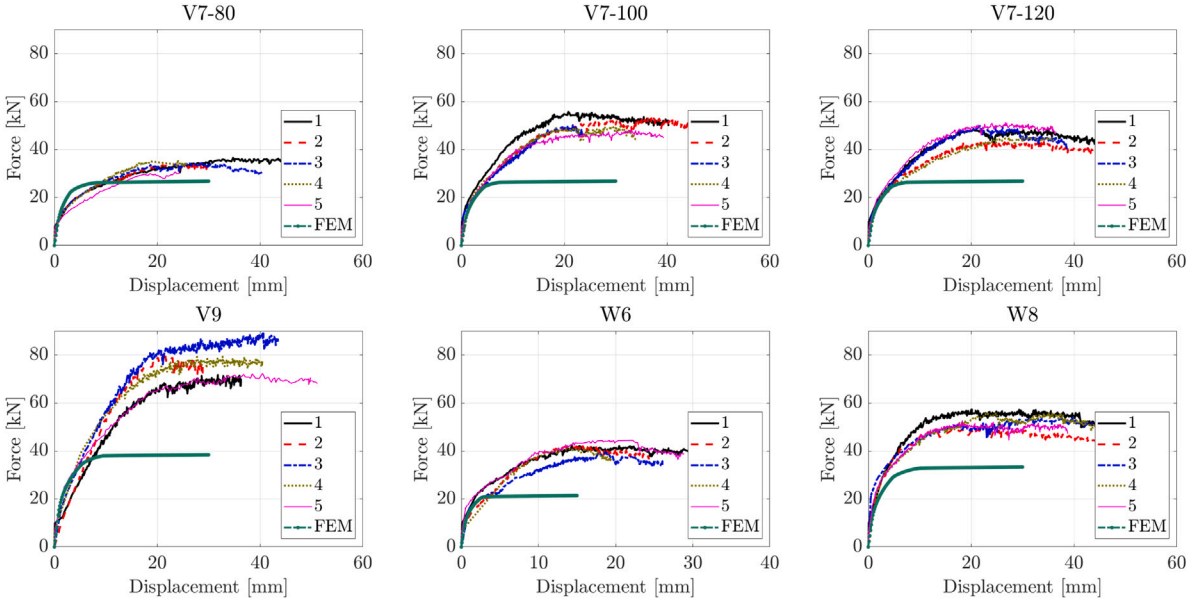

Fig. 7. Force–displacement curves for each tested configuration and comparison with FE predictions discussed in the following section.

overstrength ratio ranges between 1.7 and 2.1, with a maximum overstrength for V9 due to the higher standard deviation. The fourth block row of Table 6 shows the overstrength ratios for different reliability targets following Eq. (12). The authors also estimate the overstrength

Table 4
Shear capacity of the single fastener and of the entire connection.

Label	$R_{v,k}$ (single screw) mode (f)	No of fasteners	$R_{\mathrm{dct,an},k}$
V7-80	3.01	8	24.08
V7-100	3.46	8	27.66
V7-120	3.46	8	27.66
V9	5.07	8	40.59
W6	3.42	8	27.39
W8	4.38	8	35.04

Table 5
Mechanical parameters estimated from the experimental force–displacement curves in Fig. 7. The stiffness' is in KN/mm, the forces in kN and the displacements in mm.

No sample	$k_{el,\mathrm{exp}}$	$k_{pl,\mathrm{exp}}$	$F_{y,\mathrm{exp}}$	$v_{y,\mathrm{exp}}$	$F_{\mathrm{max,exp}}$	$v_{\mathrm{max,exp}}$	$F_{u,\mathrm{exp}}$	$v_{u,\mathrm{exp}}$	D_{exp}
V7-80									
1	7.48	0.69	21.66	2.42	36.29	39.61	34.9	48.82	20.2
2	9.04	1.18	17.94	1.65	33.89	27.75	32.8	29.48	17.91
3	8.53	1.36	17.21	1.63	34.08	23.76	30.25	38.87	23.79
4	6.4	1.3	17.94	2.26	36.64	22.66	30.88	25.51	11.3
5	7.91	1.26	13.73	1.37	30.5	23.38	29.22	23.49	17.17
V7-100									
1	9.59	2.11	29.23	2.49	54.57	21.09	49.44	39.18	15.76
2	7.16	1.77	27.55	3.13	52.73	35.67	47.89	49.23	15.72
3	7.71	2	21.93	2.22	48.95	20.41	45.57	22.88	10.32
4	9.24	1.97	23.55	2.06	48.69	27.81	42.39	33.21	18.26
5	9.48	1.95	24.58	2.09	48.69	31.5	45.43	38.21	15.24
V7-120									
1	9.56	2.03	24.14	2.04	47.67	19.83	41.02	48.74	23.85
2	12.74	1.69	22.4	1.42	43.1	20.22	38.8	43.11	30.31
3	12.65	2.05	22.94	1.43	48.32	20.07	39.89	36.26	25.29
4	10.69	1.55	22.68	1.72	44.7	26.16	43.53	28.71	16.66
5	9.32	2.08	25.68	2.25	50.61	27.64	47.2	35.02	15.56
V9									
1	8.32	2.39	35.1	3.39	71.07	33.63	68.93	35.24	10.39
2	8.28	3.37	37.02	3.57	77.11	21.29	72.83	27.34	7.66
3	9.96	3.05	41.14	3.33	85.31	39.66	82.92	42.72	12.85
4	10.91	2.73	38.85	2.87	78.15	25.01	76.89	39.05	13.59
5	8.39	1.85	37.77	3.67	70.94	35.49	68.33	50.55	13.78
W6									
1	12.89	1.97	21.74	1.39	41.83	22.05	36.89	34.38	24.74
2	6.4	2.64	20.48	2.64	41.95	13.98	36.98	24.44	9.26
3	12.17	1.62	19.09	1.29	38.65	18.1	34.3	26.27	20.38
4	9.6	2.5	18.31	1.52	40.73	14.46	35.81	19.51	12.82
5	14.68	1.97	21.28	1.16	44.12	20.11	38.29	29.05	25.12
W8									
1	10.94	3.05	28.46	2.12	57.03	32.86	48.96	48.29	22.8
2	15.11	2.81	26.04	1.44	48.96	23.21	41.31	54.72	38.03
3	19.36	2.02	28.55	1.26	53.43	34.24	46.59	51.84	41.09
4	13.32	1.77	29.32	1.88	55.37	24.39	48.31	49.31	26.27
5	13.13	2.69	26.59	1.71	51.5	18.2	47.53	38.8	22.69

ratios by assuming a log-normal probability density function. However, the difference was less than 1.5%, and the results were not reported.

As highlighted in the introduction, several pieces of research presented push-out tests on lap and spline joints between CLT elements, but none regarding the tested configuration, despite the ease of implementation. From the presented results is clear that the difference between the adoption of a normal or a log-normal distribution does not have a great influence on the final results. The overstrength ratios agree with those found in previous studies. The mean value for γ_{sc} in [48] is 1.36. Gavric et al. [48] found a more conservative value for γ_{sc} equal to 1.6 for screwed connections between panels, compared to the value of 1.3 proposed for angular brackets and hold-down loaded in shear and tension. The term γ_{an} confirms that the design model provides conservative resistance predictions. Even though there is a common agreement that this contribution should be taken into account in the calculation of the final value of γ_{Rd}, many papers do not report these values and calculate γ_{Rd} as the only contribution of γ_{sc}. Jorissen & Fragiacomo [11] obtained a mean γ_{an} equal to 1.18; Schick et al. [12] found an average γ_{an} equal to 1.43, while Gavric et al. [34] obtained 1.8. Moreover, Gavric et al. pointed out that the predictions tend to be more conservative for brittle than ductile failures.

Table 6
Evaluation of the relevant mechanical parameters for estimating the overstrength factors according to Eq. (12).

Parameter	V7-80	V7-100	V7-120	V9	W6	W8	Mean	CoV
$R_{v,k}$	24.08	27.66	27.66	40.59	26.57	34.05	30.10	0.20
$R_{\mathrm{dct,exp},m}$	34.28	50.73	46.88	76.52	41.46	53.26	50.52	0.29
σ_{exp}	2.45	2.75	2.99	5.94	1.99	3.17	3.22	0.43
$R_{\mathrm{dct,exp},0.95}$	40.76	57.98	54.76	92.20	46.72	61.64	59.01	0.30
$R_{\mathrm{dct,exp},k}$	27.80	43.47	39.00	60.84	36.20	44.88	42.03	0.26
γ_{sc}	1.47	1.33	1.40	1.52	1.29	1.37	1.40	0.06
γ_{an}	1.15	1.57	1.41	1.50	1.36	1.32	1.39	0.11
γ^*_{Rd} ($\beta = 2.64$)	1.69	2.10	1.98	2.27	1.76	1.81	1.93	0.11
γ^*_{Rd} ($\beta = 4.20$)	1.86	2.26	2.16	2.51	1.88	1.96	2.11	0.12
γ^*_{Rd} ($\beta = 3.80$)	1.81	2.21	2.11	2.44	1.85	1.92	2.06	0.12
γ^*_{Rd} ($\beta = 3.30$)	1.76	2.16	2.05	2.37	1.81	1.87	2.00	0.12
γ^*_{Rd} ($\beta = 1.75$)	1.60	2.01	1.88	2.14	1.69	1.73	1.84	0.11

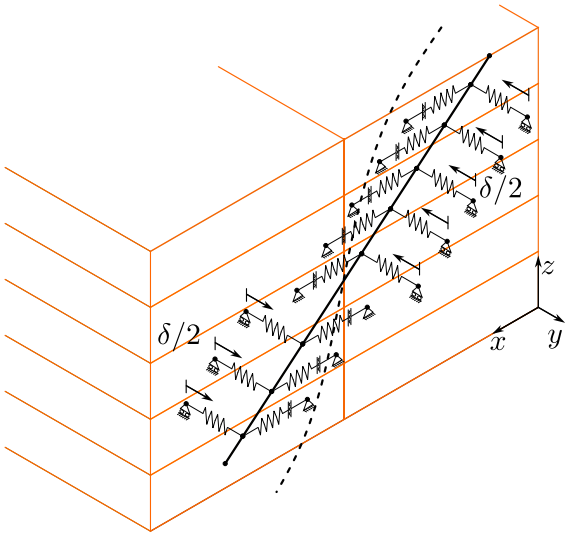

Fig. 8. Finite element model representation.

4. Nonlinear FE model

This section provides a synthetic description of the nonlinear FE model and the related capacity predictions.

4.1. Model description

To reduce the computational time required by each analysis and thus enable the execution of Montecarlo simulations, an efficient finite element model is defined. The reduced-order model of the connection consists of an assembly of mono-dimensional elements. The screw is discretized by beam elements with a solid circular section of diameter equal to 1.1 times the core diameter d_{core} to account, in an approximate way, for the thread influence on geometric properties. The CLT panels are not explicitly modelled. They are reduced, in the model, to connectors reproducing the screw-timber interaction in the embedment (Fig. 8). It is worth noting that significant transversal deformation of the screw occurs in the y axis direction. This deformation can induce appreciable second-order effects in terms of friction on the sliding plane. This mechanism, also known as the rope effect, involves the axial screw capacity increasing the resulting connection capacity

Table 7
Comparison between the experimental capacity vs the analytical and FE estimations.

Exp. Tests	Analytical model		FE model	
F_u [kN]	F_u [kN]	Relative error [%]	F_u [kN]	Relative error [%]
34.28	21.53	−37.19%	26.89	−21.55%
50.73	21.80	−57.03%	26.89	−46.98%
46.88	21.93	−53.23%	26.14	−44.25%
76.52	27.13	−64.54%	38.50	−49.68%
41.46	20.53	−50.48%	21.47	−48.21%
53.26	25.00	−53.06%	33.32	−37.43%
Mean		−52.59%		−41.35%

considerably. Therefore suitable connectors perpendicular to the sliding plane are defined, as illustrated in Fig. 8. The axial slip of the screw and the transversal deformation in the plane containing the screw and the z axis can be assumed negligible compared to transversal displacement in y direction as demonstrated by the experimental evidence in Fig. 6. The screw is assumed to behave as an ideal elastic–plastic material. The constitutive laws for connectors parallel to x and y axis (Fig. 8) depend on the timber grain-connector mutual orientation.

For connectors parallel to the grain, an elastic-perfectly plastic behaviour is assumed [49,50]. The embedment stiffness per unit of length is given by the regression formula provided in [51]:

$$k_{h,0} = -147.8d + 30.9\rho^{0.46}d^{0.68} \tag{26}$$

As highlighted in [49,50] the conventional embedment strength is approximately equal to the yielding point of the bi-linear ideal approximation of the actual embedment load–displacement curve. For connectors perpendicular to the grain, the hardening behaviour is reproduced by means of a bi-linear elastic-hardening constitutive law. The embedment stiffness per unit of length is given by the following equation descending from [51]:

$$k_{h,90} = bk_{h,0} \tag{27}$$

with $b = 0.5$. The location of the cusp in the constitutive law is the conventional embedment strength. The end of the hardening branch is assumed at a $2d$ displacement with force equal to 1.72 times the conventional embedment strength after [49,50]. The conventional embedment strength is assumed from Eq. (22). The load-to-grain angle dependence is given by the below equation given in the EC5:

$$f_{h,\alpha} = \frac{f_{h,0}}{k_{90,e}\sin^2\alpha + \cos^2\alpha} \tag{28}$$

Connectors perpendicular to the sliding plane provide a reaction in the direction of relative displacement proportional to the force acting perpendicularly to the sliding plane. This force determines the friction between CLT panels. The relative displacement between members is reproduced by assigning a displacement to the connectors parallel to y axis. A static incremental analysis mechanically and geometrically non-linear is performed.

4.2. Model validation

Table 7 compares the predicted capacity values according to the analytical model in Eq. (21) and the FE model vs the experimental observations. Fig. 7 compares the experimental and numerical curves.

The analytical and numerical models provide conservative estimations, with mean relative error equal to −53% and −41%, respectively. The model underestimates the experimental capacity, although the numerical error is nearly 10% lower than the analytical. Still, the relatively poor agreement with the experimental results will not affect the proposed procedure, including the epistemic capacity correction based on the experimental results. Discrepancies may be related to the assumed mean values for embedment strength, yielding strength and friction (Table 9). These parameters may be stock correlated and

Table 8
Experimental values of the bulk density of the CLT specimens obtained from direct weighting.

No	CLT 120	CLT 100	CLT 80
1	513.70	456.50	532.00
2	461.50	492.40	497.30
3	477.60	457.70	471.60
4	496.90	511.00	508.50
5	465.20	481.10	503.90
Mean	482.98	479.74	502.66
Std. Dev.	19.72	20.81	19.44
CoV	0.04	0.04	0.04

Table 9
Input parameters of the Monte Carlo simulations. The first value of the CoV, obtained from the experimental tests, is used to predict the $\sigma_{al}(\boldsymbol{x}_{exp}, \boldsymbol{\Theta}_{exp})$, while the second, based on the scientific literature, to predict $\sigma_{al}(\boldsymbol{x}, \boldsymbol{\Theta})$.

Symbol	Distribution	Characteristics	
ρ [kg/m^3]	Normal	$\mu = 488$	CoV = [0.04 0.1] [52]
f_y [MPa]	Normal	$\mu = 1000$	CoV = [0.01, 0.05] [52–54]
m	Normal	$\mu = 0.50$	CoV = [0.01, 0.1] [55]
α [°]	Normal	$\mu = 90$	CoV = [0.01, 0.05]

the regression formulas may not be able to predict the samples' effective properties. Moreover, the specimens have been assembled by highly specialized personnel and consequently, the assembly process results may be not representative of what codes define as the average behaviour.

The finite element model is implemented in Abaqus/Standard. The authors developed a parametric model to carry out Montecarlo analyses efficiently. Input file generation and results reading are carried out in MATLAB. The convergence of the analysis is checked from the relative displacement values. In the case of analysis, not convergent mesh and solver parameters are changed until convergence is reached.

5. Model-driven overstrength factor

According to Algorithm 1, the authors estimated the model-based partial γ^*_{Rd} using Eq. (19). Two mechanical models are compared: the analytical model in Eq. (21) and a nonlinear FE model. In the first step, the authors run an MCS to estimate the k factor in Eq. (17), where the model parameters are defined in Table 9. The first value of the CoV in Table 9 identifies the experimental test condition. The second MCS to obtain the final estimate of $\gamma_{Rd,\text{num}}$ is carried out using the second value of the CoV defined in Table 9.

Specifically, the values for ρ are obtained from the direct weighting of the CLT samples, as shown in Table 8. Conversely, CoV of the other parameters represent the upper and lower bounds according to the scientific literature. The insertion angle is deterministically assumed equal to 45° since no significant influence is expected on the basis of the consideration given in Section 4. Fig. 9 shows the histogram plots of the sampled model parameters using two values for the coefficient of variation, the lowest representative of the experimental test and the highest of the as-built connection.

However, it is essential to observe that a preliminary sensitivity analysis proved that more than 90% of the standard deviation is affected by the uncertainty of ρ. The other uncertainties do not have a significant influence on the standard deviation. Therefore, their choice can be regarded as non-influential for this research.

Table 10 collects the results of the calculations, and it is partitioned into two sections, one for the analytical and one for the FE model predictions. The forward uncertainty propagation of the parameter uncertainty through Eq. (21) leads to a significantly higher standard deviation, approximately 70% higher, except for V9. The value of k, defined in Eq. (17) ranges between 0.6 and 1.1. Additionally, the standard deviation estimated with higher values for the parameter

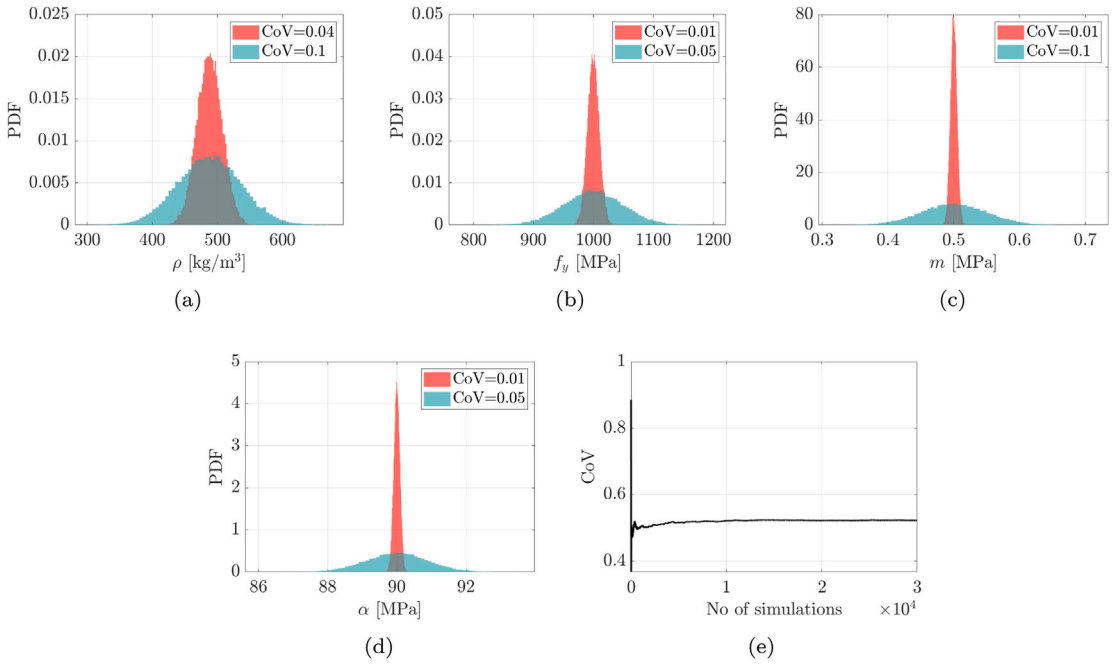

Fig. 9. (a)–(d) Histogram plots of the sampled values of the model parameters using two values for the CoV, the lowest representative of the experimental test and the highest of the as-built connection; (e) Convergence of the Montecarlo simulations in terms of the V7-80 capacity using Eq. (21).

Table 10
Estimation of the overstrength factors according to Eq. (19) using either the analytical model in Eq. (21) and the nonlinear FE model. The units are
kN.

Model	Parameter	V7-80	V7-100	V7-120	V9	W6	W8	Mean	CoV
Analytical	$E(R_{dct,mod})$	21.53	21.80	21.93	27.13	20.53	25.00	22.99	0.11
	μ_{epi}	12.75	18.56	14.32	26.19	11.62	14.00	16.24	0.33
	$\sigma_{mod}(\boldsymbol{x}_{exp}, \boldsymbol{\Theta}_{exp})$	4.27	4.30	4.31	5.34	4.04	4.92	4.53	0.11
	σ_{exp}	2.45	2.75	2.99	5.94	1.99	3.17	3.22	0.43
	k	0.58	0.64	0.69	1.11	0.49	0.64	0.69	0.31
	$\sigma_{mod}(\boldsymbol{x}, \boldsymbol{\Theta})$	11.24	11.28	11.30	13.99	10.60	12.91	11.89	0.11
	$\gamma_{Rd,mod}$ $(\beta = 1.64)$	1.86	1.89	1.77	1.94	1.53	1.55	1.76	0.10
	γ_{Rd} $(\beta = 2.64)$	1.53	1.93	1.80	2.03	1.64	1.66	1.76	0.11
	Relative error	0.22	−0.02	−0.02	−0.04	−0.06	−0.07	0.00	
Numerical	$E(R_{dct,mod})$	26.89	26.89	26.14	38.50	21.47	33.32	28.87	0.21
	μ_{epi}	7.39	23.83	20.74	38.02	19.99	19.93	21.65	0.45
	$\sigma_{mod}(\boldsymbol{x}_{exp}, \boldsymbol{\Theta}_{exp})$	1.00	1.01	0.97	1.33	0.80	1.17	1.05	0.17
	σ_{exp}	2.45	2.75	2.99	5.94	1.99	3.17	3.22	0.43
	k	2.44	2.73	3.07	4.46	2.50	2.72	2.99	0.25
	$\sigma_{mod}(\boldsymbol{x}, \boldsymbol{\Theta})$	2.69	2.68	2.62	3.62	2.24	3.19	2.84	0.17
	$\gamma_{Rd,mod}$ $(\beta = 1.64)$	1.87	2.27	2.17	2.54	1.91	1.98	2.12	0.12
	γ_{Rd} $(\beta = 2.64)$	4.46	4.19	4.63	7.22	3.78	5.25	4.92	0.25
	Relative error	−0.58	−0.46	−0.53	−0.65	−0.50	−0.62	−0.56	

uncertainties is almost 3 times the experimental one. Conversely, the forward uncertainty propagation of the parameter uncertainty through the FE model leads to a significantly lower standard deviation, yielding k values higher than 1. Therefore, it is expected that Eq. (19) provides higher overstrength factors than Eq. (12), despite the epistemic correction using k. Parallelly, it is expected that the FE model provides lower values. However, although the estimated values of the standard deviations are different between the two models, the ratios between the values corresponding to the two chosen distributions in Table 9 are quite comparable, as highlighted in Table 11. This fact proves that the rate of increment of the standard deviation is identical in the two models, despite an initial difference in the estimate. The following paragraphs show that this finding will lead to comparable overstrength factors between the analytical and numerical models.

The 7th and the 8th rows of Table 10 show the partial overstrength factors according to Eqs. (19) and (12), respectively. Interestingly, there is no substantial difference between the overstrength estimates using Eqs. (19) and (12), with a mean relative error equal to 0%.

Table 11
Comparison between the standard deviations estimated from the analytical and the numerical models. The values are in kN.

Label	Model	V7-80	V7-100	V7-120	V9	W6	W8
$\sigma_{mod}(\boldsymbol{x}_{exp}, \boldsymbol{\Theta}_{exp})$		4.27	4.30	4.31	5.34	4.04	4.92
$\sigma_{mod}(\boldsymbol{x}, \boldsymbol{\Theta})$	Analytical	11.24	11.28	11.30	13.99	10.60	12.91
Ratio		2.63	2.62	2.62	2.62	2.62	2.62
$\sigma_{mod}(\boldsymbol{x}_{exp}, \boldsymbol{\Theta}_{exp})$		1.00	1.01	0.97	1.33	0.80	1.17
$\sigma_{mod}(\boldsymbol{x}, \boldsymbol{\Theta})$	Numerical	2.69	2.68	2.62	3.62	2.24	3.19
Ratio		2.68	2.67	2.70	2.72	2.81	2.73

The analytical-based estimates are practically identical to the experimental-based ones, although the model standard deviation is significantly higher than the experimental one (see Table 11). The

Table 12
Comparison between the experimental and model-based estimations of the overstrength factors. The standard deviation values, also reported for comparison purposes, are in kN.

Label	Exp. Tests		Analytical model		FE model	
	σ_{exp}	γ_{Rd}	$k\cdot\sigma_{mod}(\boldsymbol{x},\boldsymbol{\Theta})$	$\gamma_{Rd,num}$	$k\cdot\sigma_{mod}(\boldsymbol{x},\boldsymbol{\Theta})$	$\gamma_{Rd,mod}$
V7-80	2.45	1.53	6.47	1.86	6.58	1.87
V7-100	2.75	1.93	7.22	1.89	7.33	2.27
V7-120	2.99	1.80	7.82	1.77	8.06	2.17
V9	5.94	2.03	15.56	1.94	16.13	2.54
W6	1.99	1.64	5.22	1.53	5.59	1.91
W8	3.17	1.66	8.32	1.55	8.67	1.98
Mean	3.22	1.76	8.43	1.76	8.73	2.12
CoV	0.43	0.11	0.43	0.10	0.43	0.12

reason for this stands in the calculation of the $R_{dct,exp,0.95}$ in Eq. (12) using Eq. (25), where $k_s = 2.64$ according to the [56], since the number of experimental samples equals 5. $k_s = 2.64$ is significantly higher than 1.64, which is the actual value to obtain the 95% fractile of the capacity for a normal distribution. Therefore the excellent agreement between the results in Table 10 depends on a sort of error compensation: the higher standard deviation obtained by propagating higher uncertainty values is compensated by a lower $\beta = 1.64$, used to obtain the 95% fractile of a normal distribution. Conversely, the numerator in Eq. (12) is calculated using $\beta = 2.64$, since $k_s = 2.64$ according to [56]. This fact, despite the intrinsic differences between the procedures in Eqs. (12) and (19), proves that the two estimations are in good agreement. The mean overstrength for screw connections obtained from the analytical model and the experiments is nearly 1.8. The same considerations are valid for the numerical model. The authors observe the same sort of error compensation. A higher standard deviation compensated for the higher k_s value for the 95% fractile assessment. There is a minor discrepancy between the numerical and experimental overstrength factors, whose mean values are approximately 2.1 and 1.8, respectively.

Table 12 resumes the main results of this investigation, reporting the estimations of the overstrength and the expected standard deviation net of epistemic uncertainty following the analytical and FE-based calculations. The two are compared to the experimental findings in Table 12. This study has proven that an overstrength factor between 1.8 and 2 can represent the actual uncertainties in as-built CLT-to-CLT screwed connections. The conservative value for k_s in Eq. (25) compensates for the higher uncertainty in as-built connections.

The main limitation of this research lies in the lack of experimental investigations on the role of geometric and mechanical uncertainties in the connection capacity. Conducting many tests to explore these uncertainties fully is practically infeasible due to time and resource constraints. Therefore, the authors employed a forward uncertainty propagation approach based on Monte Carlo analysis, which is a reliable method for propagating uncertainty in complex models, albeit with a computational burden. Regarding the choice of two capacity models, it is essential to acknowledge that no model can fully capture the complexity of the actual behaviour of connections. Therefore, the simplified model based on EC5 and the more advanced finite element (FE) model were selected for mutual validation and to provide a comprehensive understanding of the connection behaviour. While a three-dimensional connection model could have been developed, the computational cost of running a single analysis (which typically takes several hours) is incompatible with the Monte Carlo analyses, which involve thousands of simulations. Therefore, the proposed FE model incorporates the complex nonlinear interaction between the timber and screw while maintaining a reasonable computational burden for performing Monte Carlo analyses. Although the used models capture essential aspects of connection behaviour, they may only partially encompass all the complexities. These limitations are duly acknowledged, and future research endeavours will focus on addressing these aspects further to enhance the accuracy and comprehensiveness of the proposed methodology.

6. Conclusions

Undesired overstrength of ductile connections might compromise the expected hierarchy of failure mechanisms in CLT buildings. This paper presents an expensive experimental, analytical and numerical characterization of the overstrength of CLT-to-CLT screw connections. The experimental tests on six configurations, different in the type of screw and CLT layup, each with five repetitions, exhibited overstrength factors estimated according to [11] equal to 1.8. However, this estimate might be underestimated since the experimental tests do not represent the actual uncertainties occurring in real cases. Different wood and screw stocks are used in a real building. Additionally, the angle between the screw and the grain direction might not be precisely 45°. Therefore the authors developed a method for estimating the overstrength from a capacity model assuming more realistic values for the uncertainties of the parameters. The method is based on two Montecarlo simulations (MCS), where in the first, the authors assume the uncertainties characteristic of the experiments, and in the second one, the uncertainties typical of as-built connections. The standard deviation of the model predictions is corrected to remove the epistemic bias based on the experimental tests.

The authors used two capacity models for predicting the overstrength, one analytical proposed by the Eurocode 5 and a nonlinear FE model. Interestingly, despite the standard deviation from the MCS being significantly higher than the experiments, the model-based γ_{Rd} is in good agreement with the experimental estimates. This counterintuitive result depends on the fact that in the classical formulation in [11], the Standard [56] suggests a conservative method to estimate the 95% quantile of the resistance from the tests. It is estimated as the sum between the mean value and 2.64 times the standard deviation (not 1.64 as it should be) in the case of five test repetitions. This leads to error compensation since, in the numerical-based estimate, the 95% is obtained from the mean by summing 1.64 σ, assuming a probability density function of the distribution obtained from the MCS. This study has proven that an overstrength factor between 1.8 and 2 can represent the actual uncertainties in as-built CLT-to-CLT screwed connections.

CRediT authorship contribution statement

Angelo Aloisio: Conceptualization, Methodology, Experimental tests, Validation, Formal analysis, Investigation, Resources, Data curation, Writing – original draft, Writing and editing, Visualization, Supervision. **Yuri De Santis:** Conceptualization, Methodology, Experimental tests, Validation, Formal analysis, Investigation, Resources, Data curation, Writing – original draft, Writing and editing, Visualization, Supervision. **Dag Pasquale Pasca:** Conceptualization, Methodology, Experimental tests, Validation, Formal analysis, Investigation, Resources, Data curation, Writing – original draft, Writing and editing, Visualization, Supervision. **Massimo Fragiacomo:** Formal analysis, Supervision. **Roberto Tomasi:** Conceptualization, Methodology, Experimental tests, Data curation, Resources, Project administration, Funding acquisition, Supervision.

Declaration of competing interest

All authors have participated in (a) conception and design, or analysis and interpretation of the data; (b) drafting the article or revising it critically for important intellectual content; and (c) approval of the final version.

This manuscript has not been submitted to, nor is under review at, another journal or other publishing venue.

The authors have no affiliation with any organization with a direct or indirect financial interest in the subject matter discussed in the manuscript.

Data availability

Data will be made available on request.

References

[1] Yasumura M. Estimating seismic performance of wood-framed structures. In: Proceedings of 5th WCTE. Vol. 2, 1998, p. 564–71.

[2] Mitchell D, Paultre P. Ductility and overstrength in seismic design of reinforced concrete structures. Can J Civil Eng 1994;21(6):1049–60.

[3] Humar J, Rahgozar M. Concept of overstrength in seismic design. In: 11th world conference on earthquake engineering. Acapulco, Mexico, June. Vol. 2328, 1996.

[4] Brown J, Li M, Palermo A, Pampanin S, Sarti F. 2021, p. 13, cited By 1.

[5] Ottenhaus L-M, Li M, Smith T, Quenneville P. Mode cross-over and ductility of dowelled LVL and CLT connections under monotonic and cyclic loading. J Struct Eng (U S) 2018;144(7). http://dx.doi.org/10.1061/(ASCE)ST.1943-541X.0002074, cited By 25.

[6] Aloisio A, Boggian F, Tomasi R, Fragiacomo M. The role of the hold-down in the capacity model of LTF and CLT shear walls based on the experimental lateral response. Constr Build Mater 2021;289:123046.

[7] Tannert T, Loss C. Contemporary and novel hold-down solutions for mass timber shear walls. Buildings 2022;12(2). http://dx.doi.org/10.3390/buildings12020202, cited By 5.

[8] Chan N, Hashemi A, Zarnani P, Quenneville P. Pinching-free connector for timber structures. J Struct Eng (U S) 2021;147(5). http://dx.doi.org/10.1061/(ASCE)ST.1943-541X.0002982, cited By 7.

[9] Boggian F, Aloisio A, Tomasi R. Experimental and analytical study of Friction Connection for seismic retrofit with Cross-Laminated Timber (CLT) panels. Earthq Eng Struct Dyn 2022;51(14):3304–26.

[10] Trutalli D, Marchi L, Scotta R, Pozza L. Capacity design of traditional and innovative ductile connections for earthquake-resistant CLT structures. Bull Earthq Eng 2019;17(4):2115–36. http://dx.doi.org/10.1007/s10518-018-00536-6, cited By 28.

[11] Jorissen A, Fragiacomo M. General notes on ductility in timber structures. Eng Struct 2011;33(11):2987–97. http://dx.doi.org/10.1016/j.engstruct.2011.07.024, cited By 158.

[12] Schick M, Vogt T, Seim W. Connections and anchoring for wall and slab elements in seismic design. In: CIB working commission W18-timber structures, Vancouver, Canada. 2013.

[13] Izzi M, Casagrande D, Bezzi S, Pasca D, Follesa M, Tomasi R. Seismic behaviour of Cross-Laminated Timber structures: A state-of-the-art review. Eng Struct 2018;170:42–52.

[14] Aloisio A, Fragiacomo M. Reliability-based overstrength factors of cross-laminated timber shear walls for seismic design. Eng Struct 2021;228:111547.

[15] CEN E. 3, EuroCode 8, Design of structures for earthquake resistance—Part 3. 1998.

[16] Polastri A, Giongo I, Piazza M. An innovative connection system for cross-laminated timber structures. Struct Eng Int 2017;27(4):502–11. http://dx.doi.org/10.2749/222137917X14881937844649, cited By 29.

[17] Wright T, Li M, Moroder D, Carradine D. 2021, p. 10, cited By 1.

[18] Brandner R, Flatscher G, Ringhofer A, Schickhofer G, Thiel A. Cross laminated timber (CLT): overview and development. Eur J Wood Wood Prod 2016;74(3):331–51.

[19] Tannert T, Eng P. Design provisions for cross-laminated timber structures. In: Structures congress 2019: buildings and natural disasters. Reston, VA: American Society of Civil Engineers; 2019, p. 171–8.

[20] Hossain A, Danzig I, Tannert T. Cross-laminated timber shear connections with double-angled self-tapping screw assemblies. J Struct Eng (U S) 2016;142(11). http://dx.doi.org/10.1061/(ASCE)ST.1943-541X.0001572, cited By 83.

[21] Loss C, Hossain A, Tannert T. Simple cross-laminated timber shear connections with spatially arranged screws. Eng Struct 2018;173:340–56. http://dx.doi.org/10.1016/j.engstruct.2018.07.004, cited By 33.

[22] Dong W, Li M, Ottenhaus L-M, Lim H. Ductility and overstrength of nailed CLT hold-down connections. Eng Struct 2020;215. http://dx.doi.org/10.1016/j.engstruct.2020.110667, cited By 14.

[23] Benedetti F, Rosales V, Opazo-Vega A, Norambuena-Contreras J, Jara-Cisterna A. Experimental and numerical evaluation of hold-down connections on radiata pine Cross-Laminated-Timber shear walls: a case study in Chile. Eur J Wood Wood Prod 2019;77(1):79–92. http://dx.doi.org/10.1007/s00107-018-1365-1, cited By 15.

[24] Gavric I, Fragiacomo M, Ceccotti A. Cyclic behavior of CLT wall systems: Experimental tests and analytical prediction models. J Struct Eng 2015;141(11):04015034.

[25] Ottenhaus L-M, Li M, Smith T. Structural performance of large-scale dowelled CLT connections under monotonic and cyclic loading. Eng Struct 2018;176:41–8. http://dx.doi.org/10.1016/j.engstruct.2018.09.002, cited By 23.

[26] Ottenhaus L-M, Li M, Smith T, Quenneville P. Overstrength of dowelled clt connections under monotonic and cyclic loading. Bull Earthq Eng 2018;16(2):753–73. http://dx.doi.org/10.1007/s10518-017-0221-8, cited By 27.

[27] Zhang X, Popovski M, Tannert T. High-capacity hold-down for mass-timber buildings. Constr Build Mater 2018;164:688–703. http://dx.doi.org/10.1016/j.conbuildmat.2018.01.019, cited By 45.

[28] Ceccotti A, Sandhaas C, Okabe M, Yasumura M, Minowa C, Kawai N. SOFIE project–3D shaking table test on a seven-storey full-scale cross-laminated timber building. Earthq Eng Struct Dyn 2013;42(13):2003–21.

[29] Chen Z, Chui Y-H. Lateral load-resisting system using mass timber panel for high-rise buildings. Front Built Environ 2017;3. http://dx.doi.org/10.3389/fbuil.2017.00040, cited By 12.

[30] Connolly T, Loss C, Iqbal A, Tannert T. Feasibility study of mass-timber cores for the UBC tall wood building. Buildings 2018;8(8). http://dx.doi.org/10.3390/buildings8080098, cited By 40.

[31] van de Lindt JW, Amini MO, Rammer D, Line P, Pei S, Popovski M. Seismic performance factors for cross-laminated timber shear wall systems in the United States. J Struct Eng 2020;146(9):04020172.

[32] Sustersic I, Dujic B, Fragiacomo M. Influence of the connection modelling on the seismic behaviour of crosslam timber buildings. In: Materials and joints in timber structures: recent developments of technology. Springer; 2014, p. 677–87.

[33] Fragiacomo M, Dujic B, Sustersic I. Elastic and ductile design of multi-storey crosslam massive wooden buildings under seismic actions. Eng Struct 2011;33(11):3043–53.

[34] Gavric I, Fragiacomo M, Ceccotti A. Strength and deformation characteristics of typical X-lam connections. In: World conference on timber engineering. 2012, p. 146–55.

[35] Krauss K, Li M, Lam F. Influence of mixed-angle screw installations in CLT on the cyclic performance of commercial hold-down connections. Constr Build Mater 2023;364:129918.

[36] Brühl F. Ductility in timber structures-possibilities and requirements with regard to dowel type fasteners. 2020.

[37] Brühl F, Schänzlin J, Kuhlmann U. Ductility in timber structures: Investigations on over-strength factors. In: Materials and joints in timber structures: recent developments of technology. Springer; 2014, p. 181–90.

[38] Brown JR, Li M, Tannert T, Moroder D. Experimental study on orthogonal joints in cross-laminated timber with self-tapping screws installed with mixed angles. Eng Struct 2021;228:111560.

[39] Hossain A, Danzig I, Tannert T. Cross-laminated timber shear connections with double-angled self-tapping screw assemblies. J Struct Eng 2016;142(11):04016099.

[40] Loss C, Hossain A, Tannert T. Simple cross-laminated timber shear connections with spatially arranged screws. Eng Struct 2018;173:340–56.

[41] Hossain A, Popovski M, Tannert T. Group effects for shear connections with self-tapping screws in CLT. J Struct Eng 2019;145(8):04019068.

[42] BRANZ. Evaluation and test method EM1: Structural joints – strength and stiffness evaluation. Building Research Assn of New Zealand; 1999.

[43] Schick M, Seim W. Overstrength values for light frame timber wall elements based on reliability methods. Eng Struct 2019;185:230–42.

[44] Dietsch P, Brandner R. Self-tapping screws and threaded rods as reinforcement for structural timber elements–A state-of-the-art report. Constr Build Mater 2015;97:78–89.

[45] Blaß HJ, Uibel T. Tragfähigkeit von stiftförmigen verbindungsmitteln in brettsperrholz. 2007.

[46] Johansen K. Theory of timber connections. Theory Timber Connect 1949;9(9):249–62, cited By 501.

[47] Blaß HJ, Bejtka I, Uibel T. Tragfähigkeit von verbindungen mit selbstbohrenden holzschrauben mit vollgewinde, vol. 4, Karlsruhe, Germany: KIT Scientific Publishing; 2006.

[48] Gavric I, Fragiacomo M, Ceccotti A. Capacity seismic design of X-LAM wall systems based on connection mechanical properties. In: Meeting forty-six of the working commission w18-timber structures, CIB, international council for research and innovation. Timber Scientific Publishing-KIT Holzbau und Baukonstruktionen; 2013, p. 285–98.

[49] Schweigler M, Bader TK, Hochreiner G, Unger G, Eberhardsteiner J. Load-to-grain angle dependence of the embedment behavior of dowel-type fasteners in laminated veneer lumber. Constr Build Mater 2016;126:1020–33. http://dx.doi.org/10.1016/j.conbuildmat.2016.09.051.

[50] Schweigler M, Bader TK, Bocquet JF, Lemaître R, Sandhaas C. Embedment test analysis and data in the context of phenomenological modeling for dowelled timber joint design. In: International network on timber engineering research (INTER) - Meeting fifty-two, Tacoma (US) (INTER / 52 - 07 - 8). 2019, p. 1–17.

[51] De Santis Y, Fragiacomo M. Timber-to-timber and steel-to-timber screw connections: Derivation of the slip modulus via beam on elastic foundation model. Eng Struct 2021;244. http://dx.doi.org/10.1016/j.engstruct.2021.112798, cited By 10.

[52] Blaß HJ, Bejtka I, Uibel T. Tragfähigkeit von verbindungen mit selbstbohrenden holzschrauben mit vollgewinde, vol. 4, 2006.

[53] Ringhofer A, Augustin M, Schickhofer G. Basic steel properties of self-tapping timber screws exposed to cyclic axial loading. Constr Build Mater 2019;211:207–16. http://dx.doi.org/10.1016/j.conbuildmat.2019.03.200, URL https://www.sciencedirect.com/science/article/pii/S0950061819306907.

[54] Niebuhr P, Sieder M. High-cycle fatigue behavior of a self-tapping timber screw under axial tensile loading. J Fail Anal Prev 2020;20:580–9. http://dx.doi.org/10.1007/S11668-020-00863-4/TABLES/5, URL https://link.springer.com/article/10.1007/s11668-020-00863-4.

[55] Aurand S, Blaß HJ. Connections with inclined screws and increased shear plane friction. In: Görlacher R, editor. Proceedings - meeting 54 : 16-19 August 2021, online meeting / INTER. International Network on Timber Engineering Research; 2021, p. 147–68.

[56] EN C. 14358; Timber structures—Calculation and verification of characteristic values. Brussels, Belgium: CEN; 2016.